NAVAL POSTGRADUATE SCHOOL
Monterey, California

THESIS

SHIP TRACK CLOUD ANALYSIS FOR THE NORTH PACIFIC AREA

by

Steven Emory Morehead

September 1988

Co-Advisor Philip A. Durkee
Co-Advisor Carlyle H. Wash

Approved for public release; distribution is unlimited.

Unclassified

security classification of this page

REPORT DOCUMENTATION PAGE

1a Report Security Classification: Unclassified			1b Restrictive Markings
2a Security Classification Authority			3 Distribution Availability of Report: Approved for public release; distribution is unlimited.
2b Declassification Downgrading Schedule			
4 Performing Organization Report Number(s)			5 Monitoring Organization Report Number(s)
6a Name of Performing Organization: Naval Postgraduate School	6b Office Symbol (*if applicable*): 35		7a Name of Monitoring Organization: Naval Postgraduate School
6c Address (*city, state, and ZIP code*): Monterey, CA 93943-5000			7b Address (*city, state, and ZIP code*): Monterey, CA 93943-5000
8a Name of Funding Sponsoring Organization	8b Office Symbol (*if applicable*)		9 Procurement Instrument Identification Number
8c Address (*city, state, and ZIP code*)			10 Source of Funding Numbers: Program Element No / Project No / Task No / Work Unit Accession No

11 Title (*include security classification*): SHIP TRACK CLOUD ANALYSIS FOR THE NORTH PACIFIC AREA

12 Personal Author(s): Steven Emory Morehead

13a Type of Report	13b Time Covered	14 Date of Report (*year, month, day*)	15 Page Count
Master's Thesis	From To	September 1988	66

16 Supplementary Notation: The views expressed in this thesis are those of the author and do not reflect the official policy or position of the Department of Defense or the U.S. Government.

17 Cosati Codes			18 Subject Terms (*continue on reverse if necessary and identify by block number*)
Field	Group	Subgroup	Meteorology, Satellite Remote Sensing, Cloud Analysis

19 Abstract (*continue on reverse if necessary and identify by block number*)

Anomalous cloud lines produced by stack exhaust from ships in the North Pacific Ocean basin are analyzed. These cloud lines or "ship tracks" are observed most clearly in the channel 3 near-infrared satellite imagery obtained from the NOAA-9 AVHRR sensor. The ship tracks are produced as hot exhaust gases are expelled into the atmosphere creating an aerosol concentration higher than background areas. These aerosols serve as cloud condensation nuclei (CCN) and cause a shift in the cloud droplet distribution to a higher concentration of smaller droplets. Channel 3 AVHRR data are sensitive to cloud droplet size and show these ship tracks as an increase in radiance.

An existing ship track detection algorithm is examined and improvements are developed and evaluated. The existing algorithm works well in areas with uniform cloud cover which contain well defined ship track cloud lines. However, it begins to break down in areas with no ship tracks, cloud free areas and regions of transition from one cloud regime to another. An improved algorithm is developed which is able to improve the analysis in these problem areas. Comparison of this algorithm with the original algorithm shows a twofold increase in the percentage of valid ship tracks detected. Neither algorithm is capable of fully representing all the ship track pixels in a given image but the feasibility of this type of analysis is clearly shown. The detection algorithm is also adapted to evaluate large scale areas of data as a precursor to the development of a ship track cloud climatology for the North Pacific Ocean. While computer processing time becomes a limitation, some ability is shown for the analysis of large scale areas.

20 Distribution Availability of Abstract	21 Abstract Security Classification	
☒ unclassified unlimited ☐ same as report ☐ DTIC users	Unclassified	
22a Name of Responsible Individual: Philip A. Durkee Carlyle H. Wash	22b Telephone (*include Area code*): (408) 646-3465 2295	22c Office Symbol: 64De 64Wx

DD FORM 1473,84 MAR 83 APR edition may be used until exhausted
All other editions are obsolete

security classification of this page

Unclassified

Approved for public release; distribution is unlimited.

Ship Track Cloud Analysis for the North Pacific

by

Steven Emory Morehead
Lieutenant, United States Navy
B.S., UCLA, 1980

Submitted in partial fulfillment of the
requirements for the degree of

MASTER OF SCIENCE IN METEOROLOGY AND OCEANOGRAPHY

from the

NAVAL POSTGRADUATE SCHOOL
September 1988

Author: Steven Emory Morehead
Steven Emory Morehead

Approved by:
Philip A. Durkee, Co-Advisor

Carlyle H. Wash, Co-Advisor

Robert J. Renard, Chairman,
Department of Meteorology

Gordon E. Schacher,
Dean of Science and Engineering

ABSTRACT

Anomalous cloud lines produced by stack exhaust from ships in the North Pacific Ocean basin are analyzed. These cloud lines or "ship tracks" are observed most clearly in the channel 3 near-infrared satellite imagery obtained from the NOAA-9 AVHRR sensor. The ship tracks are produced as hot exhaust gases are expelled into the atmosphere creating an aerosol concentration higher than background areas. These aerosols serve as cloud condensation nuclei (CCN) and cause a shift in the cloud droplet distribution to a higher concentration of smaller droplets. Channel 3 AVHRR data are sensitive to cloud droplet size and show these ship tracks as an increase in radiance.

An existing ship track detection algorithm is examined and improvements are developed and evaluated. The existing algorithm works well in areas with uniform cloud cover which contain well defined ship track cloud lines. However, it begins to break down in areas with no ship tracks, cloud free areas and regions of transition from one cloud regime to another. An improved algorithm is developed which is able to improve the analysis in these problem areas. Comparison of this algorithm with the original algorithm shows a twofold increase in the percentage of valid ship tracks detected. Neither algorithm is capable of fully representing all the ship track pixels in a given image but the feasibility of this type of analysis is clearly shown. The detection algorithm is also adapted to evaluate large scale areas of data as a precursor to the development of a ship track cloud climatology for the North Pacific Ocean. While computer processing time becomes a limitation, some ability is shown for the analysis of large scale areas.

TABLE OF CONTENTS

LIST OF FIGURES

ACKNOWLEDGEMENTS

I would like to thank Mr. Doug Burks and Mr. Craig Motell of the Naval Postgraduate School Meteorology Department for their programming and problem-solving assistance. Mr Burks wrote the software for the data calibration and navigation, and Mr. Motell provided assistance in modifying the ship track detection algorithm.

Mr. Rick Kohrs and Ms. Ann Gilbert of the Naval Postgraduate School Meteorology Department provided invaluable assistance with the production of the satellite imagery and graphics used in this thesis.

Dr. James A. Coakley of the National Center for Atmospheric Research is thanked for his assistance in understanding the ship track detection technique. His work is the motivation for this thesis.

I am especially grateful to Dr. Philip A. Durkee and Dr. Carlyle H. Wash for their patience, guidance and encouragement throughout this effort. Without their support, the completion of this thesis would not have been possible.

I. INTRODUCTION

In recent years a great deal of discussion has centered around the earth's radiation budget. The Earth Radiation Budget Experiment (ERBE) was specifically designed to study this issue (Barkstrom, 1984). The controversy surrounding the greenhouse effect and its associated global warming has contributed to this discussion. As is often the case when controversy arises, speculation has progressed faster than the solid scientific understanding. It is clear, however, that the study of the radiation budget will have a very important impact on our understanding of the earth/atmosphere system.

One of the largest single factors in the earth's radiation budget is the global distribution of cloud cover. While clouds have been well understood from a mesoscale perspective for many decades, knowledge of the global variations of cloud cover as a function of time has been deficient. In the past this was primarily due to a lack of cloud data for much of the earth's surface. This is particularly true in the Southern Hemisphere and in open ocean regions where data collection is not sufficient for a comprehensive understanding of the global cloud distribution.

With the advent of satellites for the collection of meteorological data, we now have the means to examine clouds and other parameters on a global scale. The problem has now shifted from not enough data to what to do with the massive quantities of data now available. As a result there has been a great deal of development on cloud analysis algorithms as part of the International Satellite Cloud Climatology Project (ISCCP). The ISCCP is the first major project of the World Climate Research Program (WCRP) and is an effort to collect and analyze satellite radiance data in order to infer the global distribution of cloud radiative properties and to improve the modeling of cloud effects on the environment (Schiffer and Rossow, 1983). The development of a usable global cloud detection and classification algorithm is a major step toward a complete understanding the earth's radiation budget.

A. CLOUD AEROSOL DISTRIBUTIONS

Aerosols in the atmosphere have long been known to have a significant impact on the climate. Aerosol particles alter the way the atmosphere scatters and absorbs solar radiation. These processes are directly related to aerosol distribution in the atmosphere, particularly the size of the aerosols. Another way in which aerosols affect the radiation budget. is through their effect on the clouds. Coakley et al. (1987, hereafter referred to

as CBD) have theorized that the impact of aerosols on the radiation budget, due to their interaction with clouds, may be several times larger than that due to their direct interaction with the incoming solar radiation.

Although sources of aerosols are numerous, they can be divided into two categories: naturally occurring and man-made. Some of the significant natural sources of aerosol particles in marine regimes are biological producers in the ocean and sea spray resulting from turbulence at the air/sea boundary. Man-made aerosols are generally in the form of pollutants. Twomey et al. (1984) and others have documented the effects of land-based pollutants on overlying cloud layers. Twomey et al. (1968) has shown that the same type of effect can occur as a result of the exhaust from the stacks of ships at sea. These cases show areas where clouds have been generated even though the concentration of naturally occurring aerosol particles is believed to be too low to support cloud formation. An excellent example of these ship exhaust produced clouds is shown in the visible, near-infrared, and thermal infrared wavelengths (Figs. 1, 2, and 3). The visible satellite imagery (Fig. 1) shows some linear cloud lines in the clear areas. The daylight near-infrared imagery (Fig. 2) shows that these cloud features are very prominent at this wavelength. While they are not as easily seen in the thermal infrared data (Fig. 3), some evidence of them are seen in clear areas.

The importance of aerosol effects on clouds results from their serving as cloud condensation nuclei (CCN) around which cloud droplets can form. These nuclei are small enough that prior to forming into cloud droplets their interaction with incoming solar radiation is only minimal. This partially explains why it is thought that the aerosol cloud effects may be several times larger than the direct effect of the aerosol particles. The distribution and size of these aerosol particles have a monumental effect on the type and quantity of cloud formation.

B. SHIP TRACK RETRIEVAL

The concept of ship track clouds was first discussed by Twomey et al. (1968), where it was noted that there were anomalous cloud lines in satellite imagery in regions that were otherwise free of clouds. These anomalous cloud lines have been observed many times since then and now appear to fall into one of two groups. The first type is that which was observed by Twomey et al. (1968) and form in cloud free areas. While they occur often, the mechanism for their formation is not clear. The second type of anomalous cloud line arises where a ship alters the properties of a preexisting cloud mass.

Fig. 1. Visible satellite imagery showing ship exhaust produced clouds: Test case 1 at 2314 UTC on 13 July 1987.

The first effort to extract these tracks objectively from satellite data was attempted by CBD. Their algorithm searched for curvilinear cloud lines that had near-infrared (NIR) radiances in the upper 3.25% for a given region. In addition to having high NIR radiances, the ship track pixels had to be connected to at least eight other pixels also in

Fig. 2. Near-infrared satellite imagery showing ship exhaust produced clouds: Test case 1 at 2314 UTC on 13 July 1987

the highest percentile group. These criteria were to ensure that the pixels selected actually formed tracks. This ship track cloud algorithm was relatively successful at identifying tracks in regions where they were known to exist. While this study was limited to a few test cases, it did prove the feasibility of developing a track retrieval algorithm.

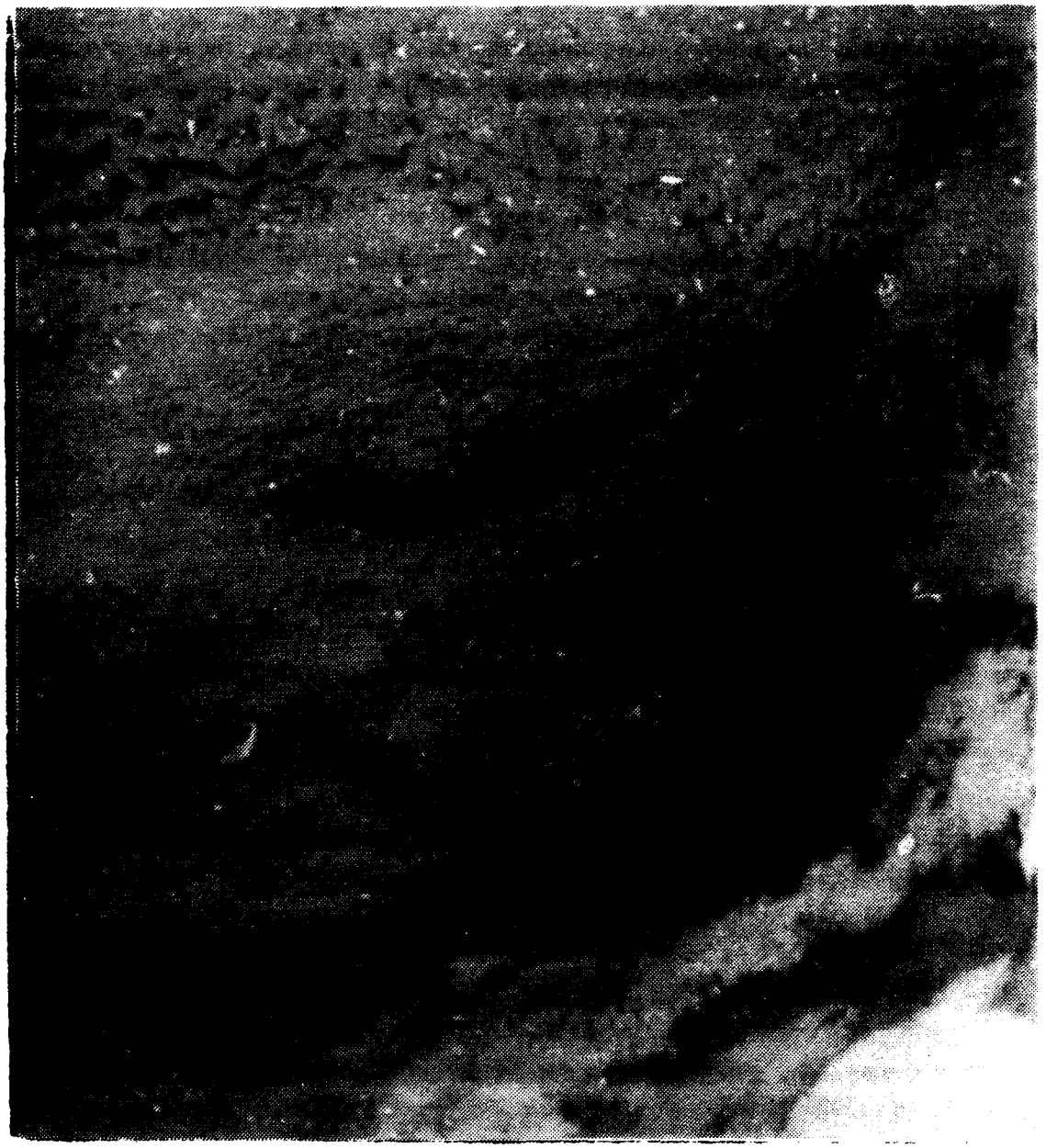

Fig. 3. Infrared satellite imagery showing ship exhaust produced clouds: Test case 1 at 2314 UTC on 13 July 1987

C. OBJECTIVES AND ORGANIZATION

The goal of this thesis is to generalize the work of CBD. This effort will have two basic objectives. The first objective is to analyze the Coakley ship track retrieval algorithm and propose improvements which make it both a more efficient and a more

accurate means of detecting ship track clouds. CBD state that ship track clouds occur only infrequently, but this may be an understatement, particularly in the summer season. The second step is to expand the ship track retrieval algorithm to operate on larger bases of data, up to and including full satellite passes. Any acceptable algorithm must be able to find and classify tracks objectively over large scale areas where the cloud properties may not be uniform over the entire area. Some problems that the current algorithm does not address are the elimination of anomalous cloud lines over land, areas that are observed to be cloud free in the visible imagery and cloud edge areas.

The theoretical background necessary for this work is presented in Chapter II and begins with a discussion of radiative transfer principles and summarizes microphysical cloud properties. Chapter II ends with a discussion of the causes of ship track cloud formation.

Chapter III will describe the data used in this study. Included will be the areas chosen for the case studies, the procurement of the data and the processing of the data accomplished before it is passed into the ship track algorithm.

The ship track retrieval algorithm will be described in detail in Chapter IV. The development of the original algorithm will be outlined and its shortcomings will be discussed. Chapter V will propose a number of improvements to the technique. The results of tests on the improved algorithm and a comparison with the abilities of the original analysis technique will also be included in Chapter V. Chapter VI will include the conclusions which are drawn from the previously mentioned results and a listing of recommendations for improvements and future work.

II. THEORY

A. DISCUSSION

Discussion of the effects of clouds on the global radiation budget requires a thorough knowledge of the physical processes governing cloud formation and the radiative processes they influence. This chapter builds the necessary theoretical framework. It will begin with a treatment of the factors important in the radiation budget and illustrate the balance of these factors. The basic principles of radiative transfer are then presented followed by basic aerosol and cloud microphysical properties. The chapter concludes with a description of the aerosol properties present when ship track clouds form.

B. THE RADIATION BUDGET

There have been numerous efforts to establish a global radiation budget since the early 1950's. Houghten et al. (1954) made the first major attempt to evaluate the radiation budget. This effort accounted for the effects of absorption by water vapor and CO_2 , and by Rayleigh scattering. The result was a set of zonally averaged albedos for the Northern Hemisphere. A much more sophisticated study was completed by Vonder Haar and Suomi (1971). They examined the reflected solar flux, the absorbed solar flux and the outgoing thermal flux at the top of the atmosphere. This effort resulted in a set of global horizontal distributions of radiation including seasonal and latitudinal variations. One of the key contributions of this study is the demonstration of deriving information regarding the radiation budget at the top of the atmosphere solely from satellite sensed data.

The two types of radiation of most interest in the radiation budget are the incoming short wave solar radiation and the outgoing long wave terrestrial radiation. Solar radiation falls into the range of 0.1 to 5.0 μm with the peak energy centered around 0.47 μm. The primary factors which affect solar radiation are the distribution of cloud cover, the latitude and the time of day. Long wave terrestrial radiation is determined by the temperature of the emitting body and temperature of the earth/atmosphere system. The resulting emission has a wavelength between 5 and 100 μm with the peak energy centered in the infrared at about 10 μm. The primary factor which affects long wave radiation is cloud which can prevent the radiation from reaching the top of the atmosphere. This large difference in energy peaks between solar and thermal infrared radiation means that these phenomena can be measured and studied separately. A representative example of

a radiation budget for a portion of the atmosphere is shown in Fig. 4. This figure shows the disposition of a scaled 100 units of incoming solar radiation as it interacts with the atmosphere. Also shown are the sources and sinks of long wave radiation which can be sensed at the top of the atmosphere.

Not shown on this figure is that the radiation budget will experience variations on daily, seasonal, and latitudinal scales. Obviously, the solar radiance is higher during daylight hours and drops to zero at night. This is not as noticeable in the infrared where the balance shows much less variability. On a seasonal basis the amount of absorbed solar radiation reaches a maximum in the summer hemisphere. On this time scale, more absorbed solar radiation will cause an increase in temperature and more emitted long wave terrestrial radiance. Latitudinally, there is much more emitted long wave radiation in the tropics and midlatitudes than farther to the north where temperature is lower. Based on some of the best methods available it appears that the best estimates for the globally averaged albedo and net outgoing long wave radiation are 31 % and 250 watts/m^2 (Henderson-Sellers, 1984).

Determining a large scale radiation budget is a complex and involved process. Some of the variables which need to be examined are: the horizontal and vertical distributions of pressure, temperature, and water vapor; the microphysical properties of the clouds; the global distribution of cloudiness for clouds with various microphysical properties; the surface albedo; the solar zenith angle; and the duration of sunlight.

Of the variables listed above, the problem of determining the global distribution of cloud cover has presented scientists with the greatest degree of difficulty. This is a major concern to researchers since the radiation budget is sensitive to the total amount of cloud cover and the properties of the clouds. Part of this difficulty is due to the lack of adequate data sources before the satellite era. While the use of satellites has solved the problem of data availability, our ability to accurately use the data is still being developed. This has been a very active research topic in recent years and has yet to result in a globally applicable and validated cloud characterization algorithm. Rossow et al. (1985) presents a comprehensive summary of the merits of many of the cloud analysis algorithms which have been proposed in conjunction with the ISCCP effort.

The impact of clouds on the radiation budget are twofold. First, clouds affect the earth's albedo which alters the amount of incoming solar radiation which is reflected by the earth/atmosphere system and returned to space. Second, an increase in the cloud cover will decrease the amount of long wave terrestrial radiation which is lost to space.

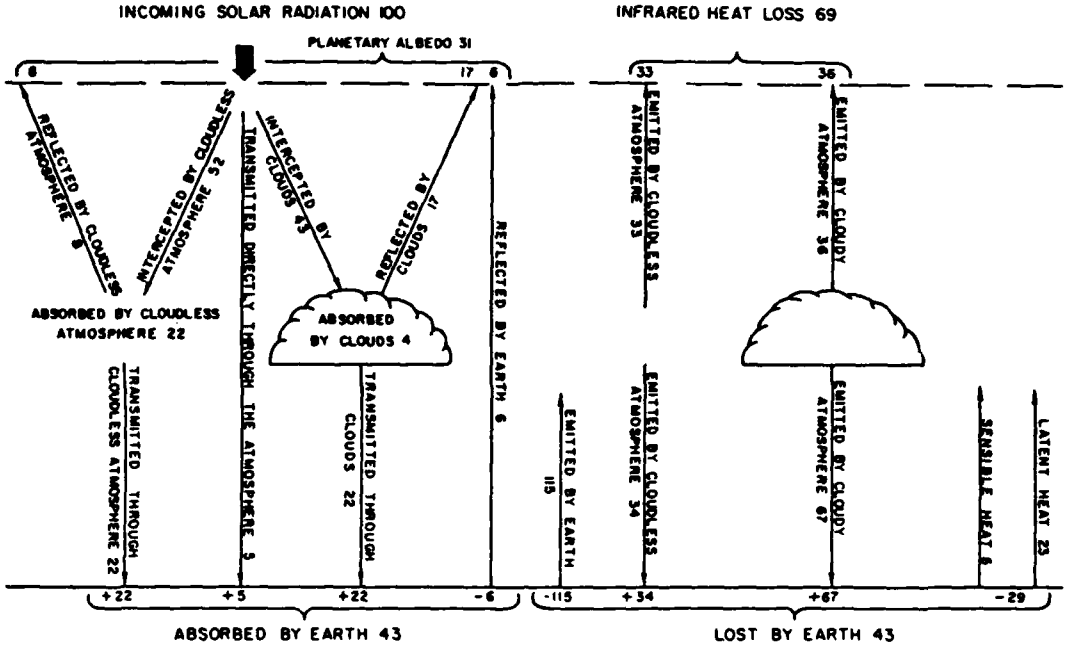

Fig. 4. Representative radiation budget: On left is the incoming short wave radiation and on the right is the outgoing long wave terrestrial radiation (after Liou, 1980)

This is primarily due to a reduced emission of long wave radiation resulting from the lower temperature associated with increased cloud cover. The interaction of these two competing processes has an important impact on the radiation budget.

C. RADIATIVE TRANSFER PRINCIPLES

A working knowledge of the principles of radiative transfer is vital to the interpretation of any remotely sensed satellite data. As stated above, the radiation budget is controlled by the proportion of short wave to long wave radiation. These radiance values are in turn controlled by the scattering and absorption interactions which occur in the atmosphere. The results of these interactions are measured at a satellite sensor in the form of emitted or reflected energy. These measurements must be converted to useful information. This conversion is possible only by understanding the total radiance received by a satellite and the proportion of the reflected energy to that resulting from thermal emission.

1. Total Radiance

The total spectral radiance measured by a satellite sensor is given by:

$$I_t(\lambda, \theta, \phi) = I_0(\lambda, \theta, \phi)e^{-\tau(\lambda)/\cos\theta} + \int_0^{\tau(\lambda)} \frac{J^*(\lambda, z, \theta, \phi)e^{-\tau(\lambda, z)/\cos\theta}}{c(\lambda, z)} \frac{d\tau}{\cos\theta}. \quad (1)$$

The first term on the the right hand side of equation 1 is the surface emitted radiance times the direct transmittance. This is a measure of the transparency of the atmosphere and represents the probability of radiation emitted by the surface reaching the top of the atmosphere. The second term on the right hand side of equation 1 represents the path radiance. This is the contribution to the total measured radiance by scattering and emission from the atmosphere at points between the surface and the satellite. The $J^*(\lambda, z, \theta, \phi)$ term is a source function which accounts for the thermal emission and scattering as given by the equation:

$$J^*(\lambda, z, \theta, \phi) = J^*_{thermal} + J^*_{scattering}. \quad (2)$$

These thermal and scattering functions are given by:

$$J^*_{thermal} = \varepsilon(\lambda, \vec{x})B(\lambda, T(\vec{x})) \quad (3)$$

and

$$J^*_{scattering} = \frac{\beta_{scat}(\lambda)P_s(\alpha^-)I_s(\lambda)e^{-\tau_s(z)/\cos\theta_0}}{4\pi}. \quad (4)$$

The $J^*_{thermal}$ term represents the contribution to total measured radiance by absorption and subsequent emission of electromagnetic energy by molecular constituents. $J^*_{scattering}$ represents the contribution due to single or multiple scattering events which result in radiant energy being directed toward the satellite sensor. These processes will be described more fully in the next section.

D. CLOUD MICROPHYSICAL PROPERTIES

Electromagnetic energy entering the atmosphere can interact by one of two processes: scattering or absorption by molecules or particles. Energy which is absorbed is converted to an increase in temperature of the absorbing body which can subsequently undergo emission. These processes represent the three classes of interactions which may

take place in an atmosphere: scattering, absorption, and emission. These three processes will cause the radiation reaching a satellite to come from one of three sources: reflection, emission, or transmission. Reflection results from energy entering the atmosphere and undergoing single or multiple scattering events until it is directed back out the top of the atmosphere. Therefore, it primarily affects short wave solar radiation. The emission source results from incoming solar radiation first being absorbed by clouds, earth and atmosphere. This absorption causes an increase in temperature which subsequently brings about emission at a multitude of wavelengths including long wave frequencies. This results in an outflux of thermal energy at the top of the atmosphere. Transmittance occurs only when radiation leaves the surface and reaches the top of the atmosphere unobstructed.

The relation of these three sources of radiant flux at the top of the atmosphere to one another will determine the dynamics of the radiation budget. They are governed by the conservation equation:

$$\varepsilon + r + t = 1, \tag{5}$$

where ε is the portion of the electromagnetic photons which are emitted by the atmosphere, r is the portion reflected and t is represents the transmitted portion. All radiant energy reaching a satellite must result from one of these processes.

1. Absorption and Emission

Atmospheric constituents will have a direct impact on satellite measured radiance as a result of absorption and subsequent emission. Absorption occurs when incoming photoelectric energy interacts with atoms and molecules raising them to an excited(and potentially unstable) state. These higher energy particles can subsequently lead to emission as the energy drops back to its more common ground state. When dropping back to the ground state, photoelectric energy is emitted at particular wavelengths. When considering emission from a simple atom, the emitted energy results in discrete wavelengths of energy. When the emitter has a more complex molecular structure, such as for water vapor, the wavelengths of emitted energy can be greatly variable.

Since clouds are composed primarily of liquid water, the absorptive properties of water are a primary concern. Liquid water absorbs electromagnetic energy at all wavelengths but at the longer infrared wavelengths the absorption is proportionally greater than at visible wavelengths. This leads to a corresponding increase in the potential for emission at longer wavelengths.

The mechanics of emission are described by the assumption of blackbody radiation. A blackbody is a perfect emitter and its emission is described by Planck's Law:

$$B_\lambda(T) = \frac{2hc^2}{\lambda^5(e^{hc/k\lambda T} - 1)}. \tag{6}$$

Planck's Law relates the emitted intensity or radiance to the wavelength and temperature of a perfect emitter. Equation 6 shows that an increase in temperature results in an increase in emission, which in turn results in a greater radiance detected by a satellite sensor.

2. Scattering

A number of models have been devised to describe scattering interactions of energy at varying wavelengths. The type of scattering which will occur is primarily dependant on the cross-sectional area of the particle with which the energy is interacting. If the scattering particles are much smaller than the wavelength of the incident radiation then the process is described by Rayleigh scattering. Rayleigh scattering depends directly on the distribution of molecular constituents in the atmosphere and as such will occur throughout the atmosphere. The direction of the resulting scatters are concentrated in the forward and backward direction as indicated in the scattering phase function diagram in Fig. 5.

In the absence of strong temperature and pressure gradients these molecular constituents causing Rayleigh scattering will vary only slightly in the horizontal. This leads the assumption that Rayleigh scattering is not a significant contributor to the horizontal variability seen in satellite images. The Rayleigh scattering efficiency is described by the relation:

$$I_\lambda \propto \frac{1}{\lambda^4}, \tag{7}$$

where I_λ represents the intensity of energy scattered in a particular direction at a particular λ. This inverse dependence on the fourth power of wavelength shows that Rayleigh scattering will not be an important contributor to the scattering for the visible and near-infrared wavelengths considered in this study.

If the scattering particle size and the wavelength of the incident energy are of the same order, then the interaction is described best by Mie scattering theory. For the types of particles in this category the scattering properties become less dependent on the

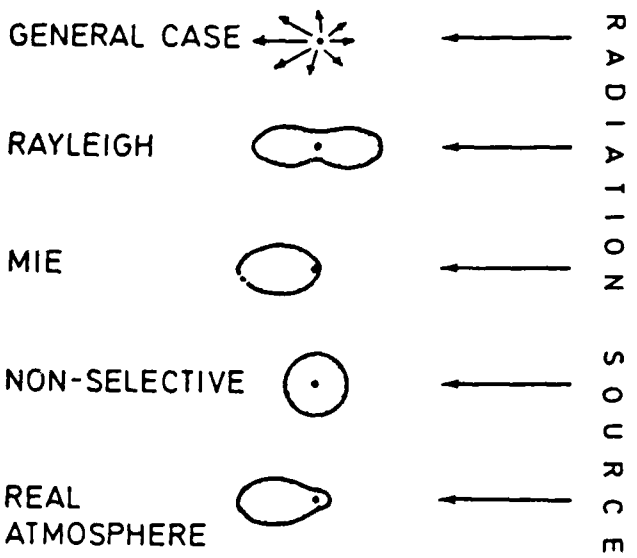

Fig. 5. Scattering phase function: for various types of scattering interactions (after Henderson-Sellers, 1984).

wavelength and more dependent on particle size. Mie scattering tends to be much more anisotropic than Rayleigh scattering in that a greater percentage of the interactions scatter in the forward direction than to the sides or backward. This is shown by the scattering phase function in Fig. 5. Under Mie scattering theory, the scattering coefficient, β_{scat}, is given by:

$$\beta_{scat} = \int_0^\infty (\pi r^2) Q_{scat}(m, r, \lambda) \frac{dN(r)}{dr} dr. \tag{8}$$

Q_{scat} is the Mie scattering efficiency of a particle with a given radius (r) and complex index of refraction (m). $dN(r)/dr$ represents the particle size distribution. From this equation it can be seen that the scattering coefficient is the product of three terms: the cross sectional area of the particle, the scattering Mie scattering efficiency, and the size

distribution of the particles. These three components are illustrated in Fig. 6 for a distribution of particle sizes and a wavelength of 0.6943 μm.

From Fig. 6b it is apparent that the value of the Mie scattering efficiency approaches a constant value near 2 for $\lambda = 0.6943$ μm, hence losing its dependence on particle size. This represents the region where Mie theory is no longer valid and scattering is described by geometric optics. For these particles whose areas are much larger than the wavelength of the incident energy, scattering is relatively independent of both wavelength and particle size.

3. Reflectance

In this study we are considering reflectance from cloud surfaces. At the wavelengths used, the reflectance depends most heavily on the Mie scattering mechanisms described above. To get a useful measure of the degree of scattering we examine the optical depth which is defined by:

$$\tau = \int_0^H \beta_{scat}(\lambda) dz, \tag{9}$$

where H is the altitude of the satellite sensor. This equation provides a measure of the scattering potential of the cloud layer.

The reflectivity of a cloud mass is also dependent on the phase function of the scattering interactions occurring in the cloud. As shown in Fig. 6 the different types of scattering interactions will have very different directional characteristics. Also, for a given type of scattering the phase function will vary with wavelength and particle size. In Mie scattering, the majority of the scatters occur in the forward direction. As particle size increases even more forward scattering occurs. Hunt (1972) describes the phase scattering characteristics as well as the particle size effects on the reflectance of cloud layers in the visible and infrared windows. This study showed that the changes in cloud radiative properties seen at visible and infrared wavelengths are consistent with changes in the size distribution of particles.

4. Aerosol Distributions

The size distribution of aerosol particles in the atmosphere covers a wide range. At the low end of the scale are cloud condensation nuclei (CCN) which typically have a radius on the order of 0.1 μm. As size increases, cloud droplets form which commonly have radii on the order of 10 μm. A large cloud droplet can have a radius up to 100 μm and a rain droplet would be even larger. Many of the interactions mentioned in the

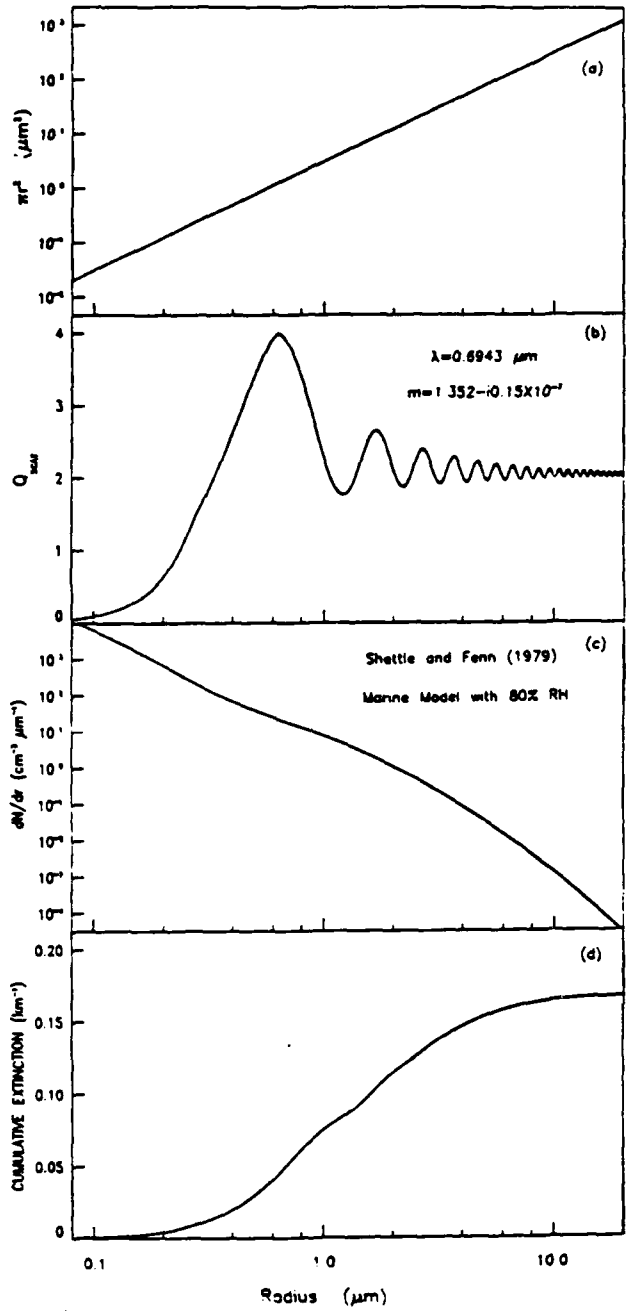

Fig. 6. **The terms from the scattering coefficient of equation 9:** (a) the cross sectional area, (b) the Mie scattering efficiency , (c) a representative particle size distribution after Shettle and Fenn (1979), and (d) The cumulative scattering coefficient, all as a function of radius (after Durkee, 1984).

above section have a strong dependence on the distribution of these aerosol particles in both size and concentration.

While there are numerous sources of aerosols in the atmosphere, the source we are most concerned with here is ships at sea. These ships expel exhaust into the environment in the form of water vapor, gaseous constituents and aerosol particles. Additionally, the gaseous constituents can condense providing an additional source of aerosol particles. These aerosols are of a size where they can function as CCN and they boost the CCN concentration to far above naturally occurring values. Hindman et al. (1977) shows that the concentration and size distribution of CCN has a direct impact on the formation of cloud droplets. Knowing that cloud droplet distribution will depend on the distribution of the CCN, it follows that this new source of CCN will cause a change in the reflective properties of the clouds. This process was illustrated in Twomey and Cocks (1982). Also shown was that the increase in the droplet concentration will be accompanied by a decrease in the size of the droplets. This is necessary since the ship exhaust does not significantly alter the equivalent liquid water content for a given volume of atmosphere. The shift in droplet size downward toward the visible and near-infrared wavelengths coupled with the increase in concentration will result in a significant increase in the reflectance due to scattering. Twomey (1977) observed this effect of increased reflectance due to an increase in the number of small size CCN.

E. SHIP EXHAUST PRODUCED CLOUDS

Anomalous cloud lines are curvilinear cloud formations which appear in visible and near-infrared satellite imagery. They are likely to appear throughout the year but are most commonly seen in summer months when their frequency of occurrence follows the increase in stratus cloud mass. The cloud lines have the appearance of a cloud plume in that they are narrow at the source and tend to disperse horizontally with increased distance from the source. They can be seen in satellite imagery for periods of up to several days and can be tracked as they are moved by synoptic-scale winds.

From an examination of visible and infrared satellite imagery it appears that there are two different types of anomalous cloud lines. First, there are those which are observed to form in regions that were previously cloud free. These cloud lines have been observed for many years but the mechanism of their formation is not fully understood. The second type are those generated in cloudy areas and observed because changes in the microphysical properties of the clouds are detectable in the near-infrared satellite imagery. This occurs because of the shift to a smaller size cloud droplet distribution

resulting from the addition of small CCN. Conover (1969) first identified the source of these anomalous cloud lines as exhaust coming from the stacks of ships transiting at sea. The ship exhaust can be expected to have different temperature, moisture, and aerosol concentrations than the surrounding air mass. Variations in the moisture content are minimal and appear to be insufficient to cause cloud formation by themselves. The increase in the temperature of the exhaust is significant but is not vital to the existence of these anomalous cloud lines. As stated, the ship track cloud lines have been observed to exist for several days. The hot exhaust gases will reach thermal equilibrium long before several days have transpired. This was confirmed by Stern et al. (1973) who used the Davidson-Bryant plume rise formula to calculate that a 600 K exhaust plume will reach thermal equilibrium after rising approximately 50 meters. This leads to the assumption that the most likely cause of the ship track clouds is the increased aerosol content produced by the ship exhaust (Conover, 1969).

Fett et al. (1979) have indicated that the most common area of formation of the anomalous cloud lines lie in regions where closed cellular clouds with medium base heights (3-6km). Within these regions, areas of anticyclonic activity create an inversion which serves to lower the height of the marine layer to below the level of the closed cellular clouds. When this occurs, the closed cellular clouds often become scattered or broken stratus which appear as an open cellular pattern in the satellite imagery. Also, fog and haze are often reported in areas where cloud lines form, which indicates a high relative humidity. Some other conditions which help to promote the formation of ship track clouds are saturated or supersaturated air near the top of the marine boundary layer, an air temperature which is cooler than the sea-surface temperature, and a minimum of vertical wind shear. Saturated air at the top of the boundary layer provides sufficient moisture to form cloud droplets in the presence of the increase of CCN provided by the ship exhaust. Ship track cloud formation will be further enhanced if the boundary layer is capped by a strong inversion with warm dry air aloft. The warm sea surface temperature enhances track formation in the presence of a moist boundary layer by creating an environment which is more favorable to fog and haze. The effect of wind shear in the boundary layer would be to disperse the CCN provided by the exhaust resulting in poorly defined or nonexistent cloud lines.

Fig. 7 from Fett et al. (1979) shows a representation of the formation of an anomalous cloud line as a function of time after the passage of a ship. In the first frame, hot exhaust gases are expelled into the atmosphere. These gases are rich in CCN and

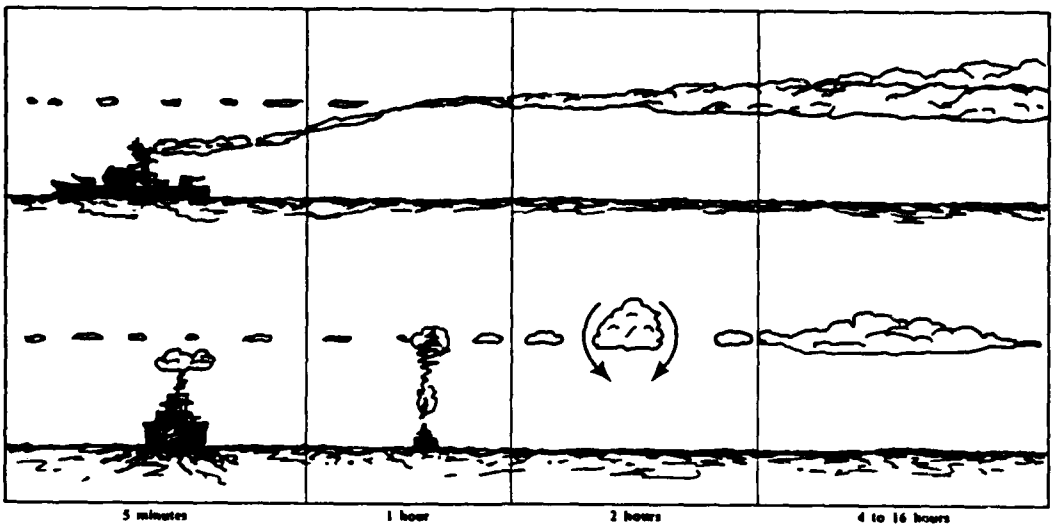

Fig. 7. The formation of a ship track cloud as a ship transits the area: (after Fett, 1979).

initially carried aloft by the buoyancy created by their greater temperature. The second frame shows the CCN rich air reaching the top of the marine boundary layer. By this time the exhaust is likely reaching thermal equilibrium as it nears the lifting condensation level where cloud formation can occur. As condensation occurs at the CCN, latent heat is released which increases convective activity which promotes cloud line formation. The third frame shows a well defined cloud line caused by continued addition of CCN and increased convective activity. The final frame shows the cloud line beginning to disperse since the CCN rich effluents are no longer being supplied to the area. This causes reduced latent heat release which in turn decreases the convective activity.

In summary, anomalous cloud lines can form in areas where relatively stagnant conditions and a low moist marine boundary layer exist. The clouds result from CCN supplied by ship exhaust. They can be observed in both the visible and near infrared satellite imagery as changes in the radiance due to altered properties within the clouds.

III. DATA AND SIGNAL PROCESSING

Chapter III describes the satellite platform and sensor used to collect the data for this study. The source and format of the data will be discussed as will the basic signal processing and calibration which is conducted prior to the use by the ship track cloud retrieval algorithm. A listing of the test cases chosen for this study, including the reasons for the selection of each, is deferred to Chapter V.

A. THE SATELLITE

The satellite platform used was the NOAA series polar orbiting satellite. These satellites are sponsored by the National Oceanographic and Atmospheric Administration and are intended to provide both scientific researchers and operational users with ocean and atmosphere measurements. These satellites fly in a sun-synchronous polar orbit at an altitude of approximately 525 nautical miles.

There are generally two NOAA series satellites flying at any given time. The advantage of having two platforms is that they can be placed in orbit such that they provide sensor coverage at different times of day. The platforms currently in use are NOAA-9, which was launched in December 1984, and NOAA-10, which was launched in September 1986. The next operational launch of a NOAA series satellite is scheduled for the fall 1988 timeframe. These satellites are expected to continue to provide data into the mid 1990's.

B. THE SENSOR

On board the NOAA satellites, radiance data are collected by the Advanced Very High Resolution Radiometer (AVHRR) instrument. This sensor will give a resolution of approximately 1 km by 1 km from the 525 n mi altitude of a polar orbit.

The AVHRR sensor records radiance measurements in each of five wavebands as shown in Table 1. As can be seen from the table, channels 1 and 2 are in the visible, channel 3 is near-infrared, and channels 4 and 5 are in the infrared portion of the electromagnetic spectrum.

TABLE 1 Wavebands of the Advanced Very High Resolution Radiometer (AVHRR)		
Channel	Wavebands(μm)	Center Frequency(μm)
1	0.58 - 0.68	0.63
2	0.725 - 1.10	0.83
3	3.55 - 3.93	3.7
4	10.3 - 11.3	11
5	11.5 -12.5	12

The channels which are used in the detection of ship track tracks are 1, 3, and 4. The most important information is contained in the channel 3 imagery since ship track clouds not detectable at other wavelengths are often easily seen in this channel. The visible imagery is important because we know that ship track clouds are not likely to exist in regions which are cloud free in the visible. This channel also provides some information which is vital to the classification of cloud type and determining the microphysical properties of the clouds. While ship track clouds are not generally seen in the infrared, channel 4 imagery can be used to help classify cloud masses. Channel 4 is also used to help locate non ship track pixels which have similar microphysical properties to nearby ship track pixels.

C. SIGNAL PROCESSING AND CALIBRATION

The data collected by the NOAA satellites are transmitted to a ground station operated by the Scripps Institution of Oceanography in La Jolla, California. The original data comes on the tapes in the form of counts of radiant energy in each of the five channels mentioned above. In order to use the data, they must first be converted to a usable unit by some type of calibration. The discussion here will be limited to channels 1, 3, and 4 as they provide the data of interest in this study.

1. Channel 1

The AVHRR channel 1 data are calibrated assuming a linear relationship between the counts received by the sensor and the reflectance. This calibration is done in terms of albedo and is described by Allen (1987). The calibration results in units of percent reflectance.

2. Channel 4

The channel 4 data result almost exclusively from thermal emission. Using a linear correlation to counts, this channel is converted to a radiance measurement with the units of W/m^2-sr-cm^{-1} .

3. Channel 3

Since the AVHRR channel 3 is in the near-infrared band, it is comprised of both reflectance and thermal emittance information for daylight passes. Two types of channel 3 data will be used in this thesis: (1) a channel 3 radiance which contains both the reflectance and emission contributions and (2) a channel 3 reflectance signature which represents only the portion of the measured irradiance resulting from reflectance. The first is determined based on a linear correlation between counts measured and radiance. The resultant units of radiance are W/m^2-sr-cm^{-1} The channel 3 reflectance is derived from the channel 3 radiance just described and the channel 4 data. The channel 4 data are used to represent the thermal emission and are subtracted from channel 3, leaving only a reflectance. This procedure is described fully by Allen (1987).

IV. THE ANALYSIS ALGORITHM

As illustrated by Fig. 3 it is easy to look at the channel 3 AVHRR imagery and select cloud features which appear to be the result of ship tracks. The wider and older tracks can sometimes be seen in the channel 1 imagery (Fig. 1). While manual identification could be used, it is not the most desirable approach since it is based on the judgement of the observer examining the imagery. This leads to the desirability of developing an automated analysis algorithm which is able to detect and classify the ship track cloud features.

The use of an automated analysis technique is needed for a number of reasons. It will allow the quantity of data examined to be greatly expanded. It will also permit all data to be examined under the same standards, thereby removing the subjectivity involved when human intervention is required. This is particularly advantageous when considering the results from a historical perspective. Another advantage is that once the ship track clouds are identified, they can be immediately studied statistically. This is useful for validating the success of the analysis technique and for assisting in the classification of both ship track and background cloud masses.

A. THE COAKLEY ANALYSIS TECHNIQUE

The first attempt at a ship track algorithm was made by CBD. This algorithm is a logical starting point for the development of a more globally usable technique. CBD made several important contributions to the understanding of ship track cloud formation. By examining the NIR radiance, anomalous cloud line areas were found to have a significantly higher 3.7 μm radiance than surrounding unperturbed clouds having similar thermal properties. This was linked to the increase in smaller sized cloud droplets relative to larger droplets as a result of the CCN rich ship exhaust. The ship tracks also had an increased average visible reflectance. Assuming a relatively constant water vapor content, the shift to smaller droplet sizes would have to be accompanied by an increase in the number of droplets. This causes an increase in the scattering at visible wavelengths and is seen as a greater AVHRR channel 1 reflectance. This increase in reflectance is not always observable because the cloud thickness is generally sufficient to cause the visible imagery to be highly reflective.

At infrared wavelengths, liquid water is a strong absorber. The result is that channel 4 of the AVHRR detects thermal emission by clouds. However, since we know that ship

exhaust reaches thermal equilibrium quickly, ship tracks are observed in channel 4 only in regions where the cloud is produced by the ship and is also observable at visible wavelengths. These findings are supported by Fig. 8 which shows the channel 1 reflectance, and channel 3 and 4 radiances for ship track and non-perturbed clouds plotted against one another. This figure, which is from data examined by CBD, shows that visible reflectance and NIR radiance values are higher in the ship track group than the unperturbed or control group. Additionally, we can see that the increase in the NIR is much more marked than in the visible. This is expected since some areas are already highly reflective in the visible and the addition of more scattering water droplets will not produce a noticeable effect on the reflectivity. The figure also shows that the reflectances and radiance values show a great deal of variability in both the ship track and control groups. CBD attribute this to large variations in the distribution and size of cloud droplets within the same cloud mass. This is a very important result since it serves to obscure some of the increase in the channel 1 reflectivity.

The Coakley algorithm uses the channel 3 data as the primary means of detecting the ship track clouds since this channel shows the largest response to their presence. To select pixels which are believed to be the result of ship tracks the algorithm starts with a 512 X 512 full resolution satellite image and divides it into 64 X 64 pixel subframes. Since the resolution of the AVHRR instrument is approximately 1 km, these subframes represent a 64 square kilometer area. This size subframe is chosen as an area within which the cloud masses should exhibit similar radiative properties. Within these subregions the channel 3 radiance values are ordered and the top 3.25% are designated as potential ship tracks. These pixels are then compared to their neighboring pixels in an attempt to discover the linear features expected in ship track clouds. If a pixel is connected to at least eight others in the top 3.25% then it is considered to be a ship track cloud.

The Coakley algorithm produced a number of output products used for the evaluation of the ship tracks. These include:

- An output file containing satellite and processing parameters. This is primarily used as a means of displaying information regarding the use of the technique.
- Plots showing a comparison of the channel 1, 3, and 4 reflectance/radiances for both ship track and control group pixels. Fig. 8 is an example of one of these plots.
- A file of data to be used for statistical analysis. These data include such information as the number of ship tracks, mean radiance values and standard deviations, solar zenith angle, etc.

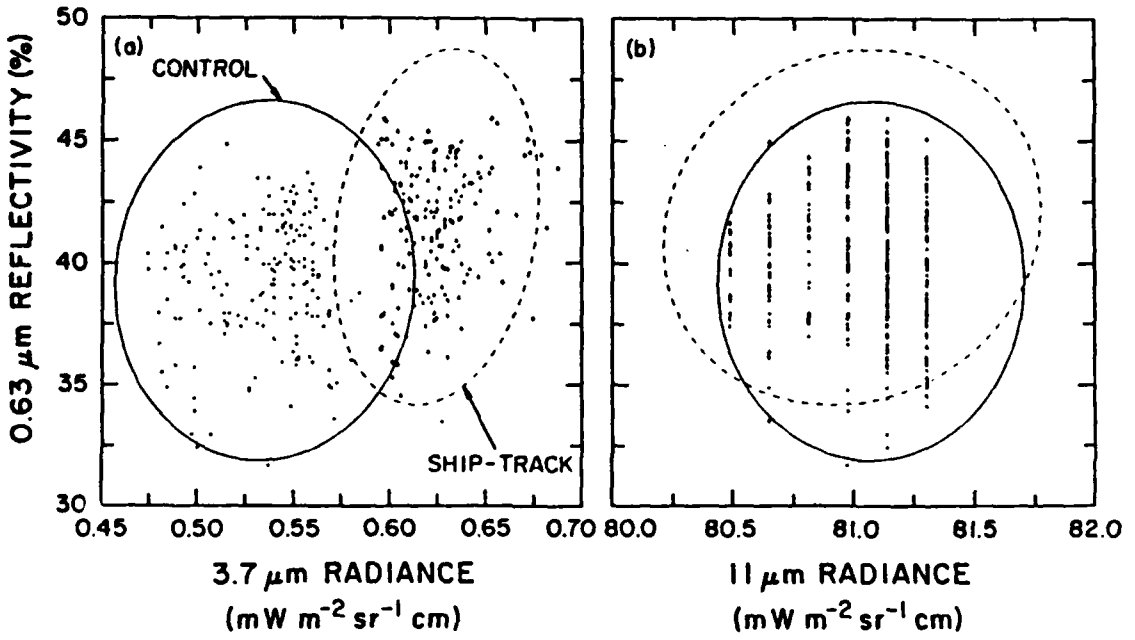

Fig. 8. Distributions of 0.63 μm reflectivity as a function of: (A) 3.7 μm radiance and (B) 11 μm radiance for a ship track cloud and a nearby unperturbed cloud mass with similar properties (from Coakley et. al., 1987)

- A 512 X 512 image showing the pixels that are selected as ship tracks.
- a mask of randomly selected non-perturbed pixels to be used as control group for comparison with the ship track pixels. These random pixels are selected only if they have channel 4 radiances similar to those of the ship track pixels.

In terms of evaluating the success of the algorithm on a subscene by subscene basis, the ship track pixel image is the easiest to interpret. When compared to the channel 3 imagery for the same area it provides immediate feedback on which tracks are detected and which are not. The plots showing the radiance and reflectance values are useful in that they are able to show that there is a quantifiable difference in the properties of ship track and control group pixels. The purpose of the statistical data file is to provide a measure of validation for the technique as more and more ship tracks are examined.

The Coakley algorithm was very successful as a first attempt at detecting ship track clouds with an automated technique. In CBD it was applied to satellite data from each of four days which were known to have ship tracks. These four days of data were narrowed to an examination of only those tracks which were imbedded in large scale stratus

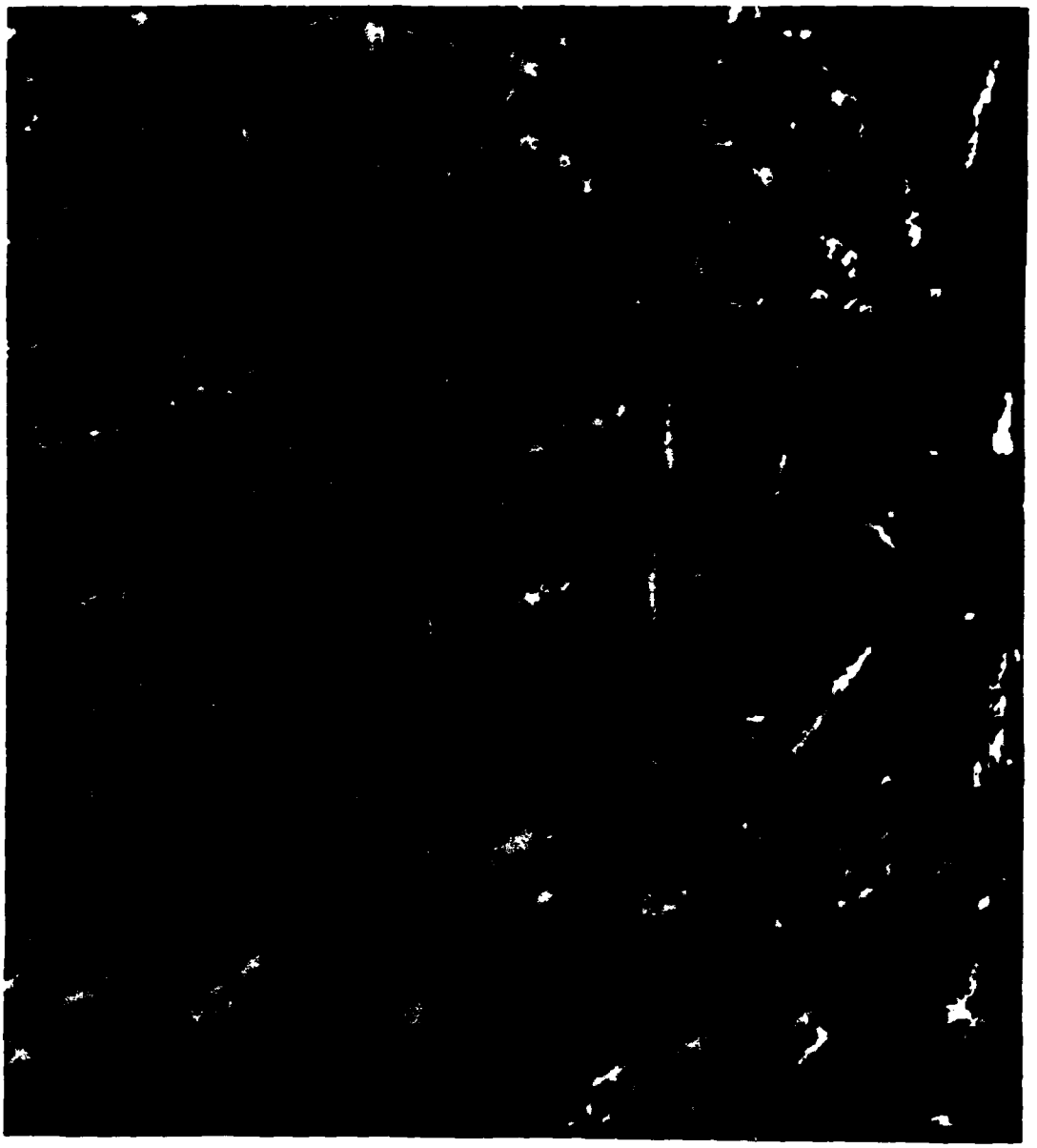

Fig. 9. Ship track pixel image produced by the Coakley algorithm: Area represented is test case 1 from 2314 UTC on 13 July 1987.

or stratocumulus cloud masses and where the ship track clouds and nearby non-perturbed clouds had similar properties at thermal infrared wavelengths. With these restrictions, the algorithm was able to determine the location of ship track pixels with reasonable accuracy. Fig. 9, Fig. 10 and Fig. 11 are examples of the application of the

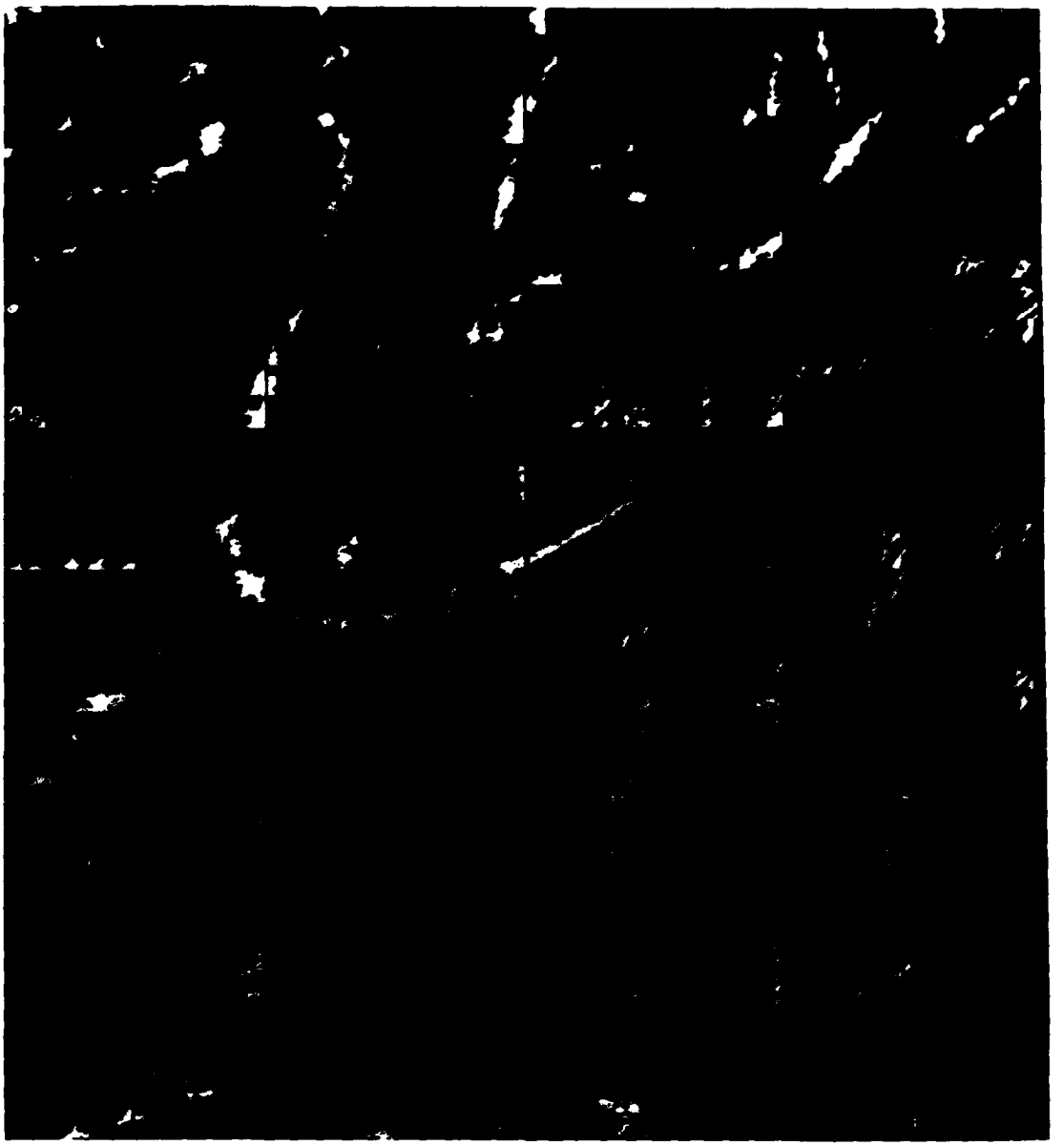

Fig. 10. Ship track pixel image produced by the Coakley algorithm: Area represented is test case 2 from 2314 UTC on 13 July 1987.

Coakley algorithm to three areas in the North Pacific Ocean basin. These same areas will be used later for evaluating the performance of the improved ship track detection algorithm. Additionally CBD were able to statistically document the increase in channel

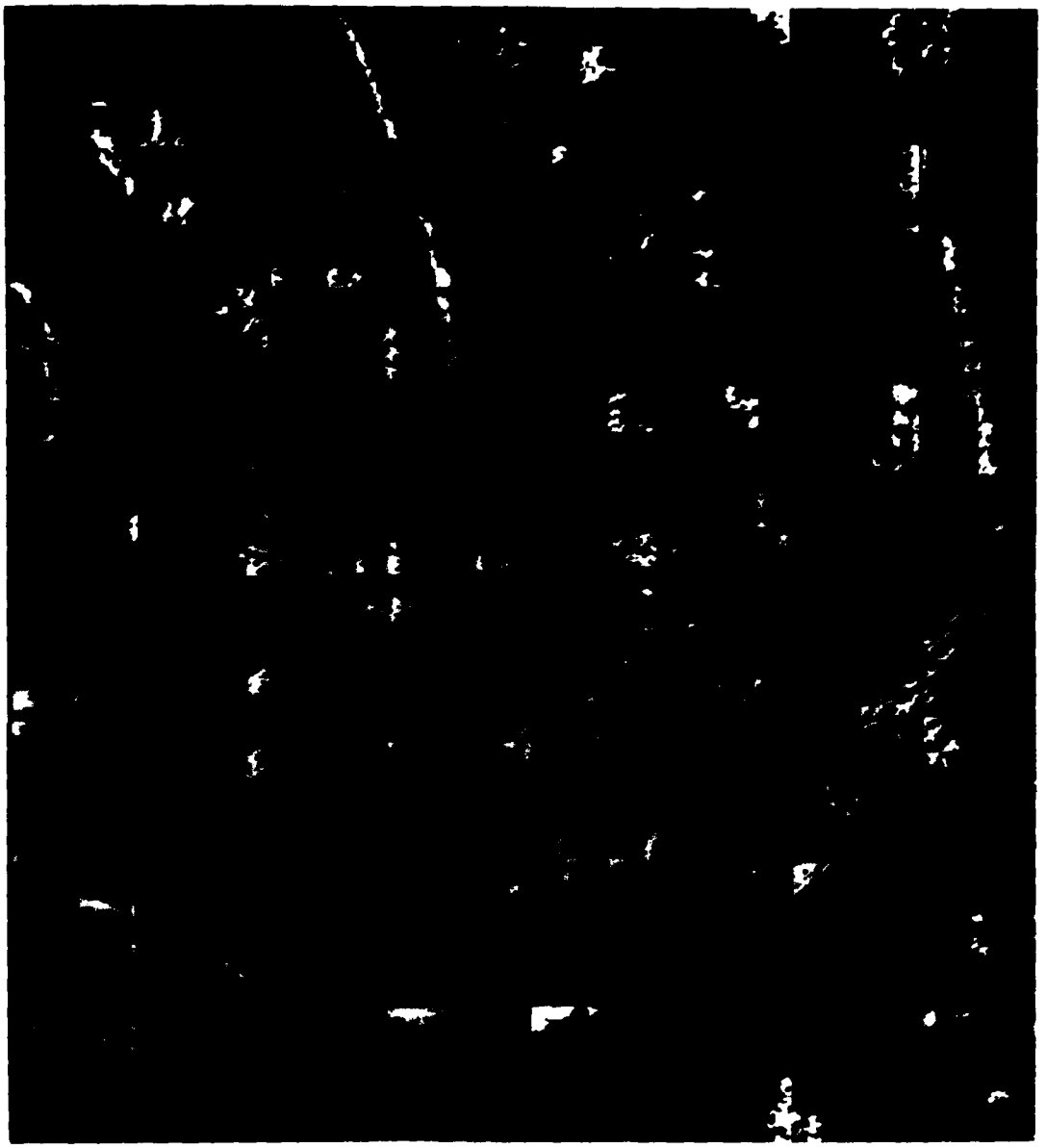

Fig. 11. Ship track pixel image produced by the Coakley algorithm: Area represented is test case 3 from 2314 UTC on 13 July 1987.

I reflectance and channel 3 radiance in the presence of ship track clouds as shown by Fig. 8.

However, the technique is subject to some shortcomings which restrict its use for a large scale analysis or climatology of ship tracks. The algorithm was applied to cases

that were easy to analyze and did not subject the technique to varying types of cloud masses. The highest percentile pixels for each subframe are selected as potential ship tracks even if no tracks are present in the subframe. This leaves only the line segment test to eliminate these erroneous pixels. As a result, when the algorithm is applied to a subframe which is known to be free of ship tracks, the results are quite disappointing. This problem was bypassed in CBD by examining areas known to contain tracks.

A different problem often arose in subframes that contained several (or very large) ship tracks. In these cases the highest 3.25% of the pixels was insufficient to represent all of the ship track clouds. This results in large gaps in the structure of the ship track imagery. Another shortcoming of the algorithm was its inability to correctly and accurately interpret the over land areas and oceanic areas which are cloud free. Any globally usable technique must be able to cope with these types of areas.

Probably the most significant drawback to the successful application of the Coakley algorithm to large scale areas is the limitation on computer processing time. The computations required by the algorithm are such that each 512 X 512 subscene of data requires several hours of processing time. An AVHRR data pass covering a large scale area of the North Pacific Ocean basin contains 28 or more subscenes so computer run time becomes a serious concern. Reduction of the processing time required will be an important goal in the development of a global analysis scheme.

V. RESULTS

A. THE TEST CASES

The test cases examined were selected based on the presence of ship tracks, availability of data, and the measure of challenge to the analysis technique. The three test cases considered were taken from the NOAA-9 satellite pass at 2314 UTC on 13 July 1987. This pass is interesting in that it not only has a great deal of ship tracks, but they are found in areas of the pass that are widely separated. The cloud characteristics in the vicinity of each of the cases are different and present different challenges to the ship track retrieval algorithm. An overview of this satellite pass is shown in Fig. 12. This overview shows the position of the test cases relative to each other and indicates the relative size of the 512 km by 512 km areas being examined.

Case 1 covers a region near the eastern edge of the satellite pass. This area is confined by the latitude range 39° 46.2′N to 42° 27.4′N and the longitude range 132° 27.1′W to 143° 09.1′W. The channel 1, 3 and 4 satellite imagery for this case were presented earlier as Figs. 1, 2 and 3.

The area examined by case 2 is to the northwest of the first case. It is bounded by 40° 56.6′N to 44° 59.5′N latitude and 126° 21.6′W to 133° 21.1′W longitude. The channel 1, 3, and 4 satellite imagery is given by Figs. 13, 14 and 15.

The third case is off the coast of Baja California, well to the south of the first two cases. It is bounded on the north and south by 21° 06.2′N and 25° 24.0′N. The east-west limits extend from 120° 14.1′W to 125° 39.4′W. Figs. 16, 17 and 18 present the channel 1, 3, and 4 satellite imagery for this case.

B. THE ALGORITHM MODIFICATIONS

This section will present proposed solutions to some of the shortcomings of the Coakley ship track retrieval algorithm developed in CBD. The approach used is to utilize the basic framework of the existing technique and add additional selection criteria to deal with the specific problems noted in the previous chapter. Each of these improvements then will be applied to the test cases to assess their merits and deficiencies. The additional test criteria added to the algorithm are:

1. channel 4 variance test,
2. channel 1 threshold test,

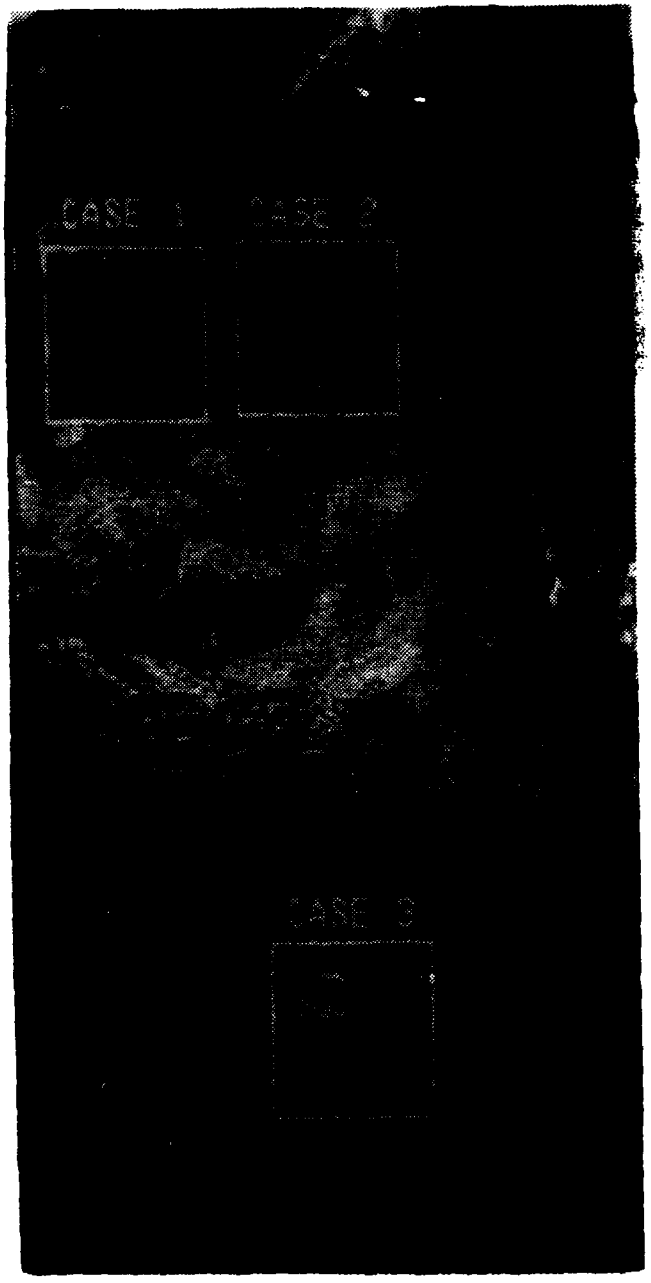

Fig. 12. Channel 2 overview of the NOAA-9 satellite pass AR6105: pass occurred at 2314 UTC on 13 July 1987 and shows the three test cases studied in this thesis.

Fig. 13. Case 2 visible channel 1 satellite imagery: 2314 UTC on 13 July 1987

3. channel 3 threshold test,
4. variations to the number of pixels considered to be a significant line segment,
5. altering the percentile value used for selecting the potential ship track pixels, and
6. the use of a reflected channel 3 signature rather that the raw radiance value currently used.

Fig. 14. Case 2 near-infrared channel 3 satellite imagery: 2314 UTC on 13 July 1987

The first five proposed improvements described above can be applied to the algorithm at the same time. This allows the best value for each of the thresholds and parameters to be selected and used in conjunction with each other. Fig. 19 shows, in flow chart format, how each of the tests used enters into the algorithm. If the near-infrared

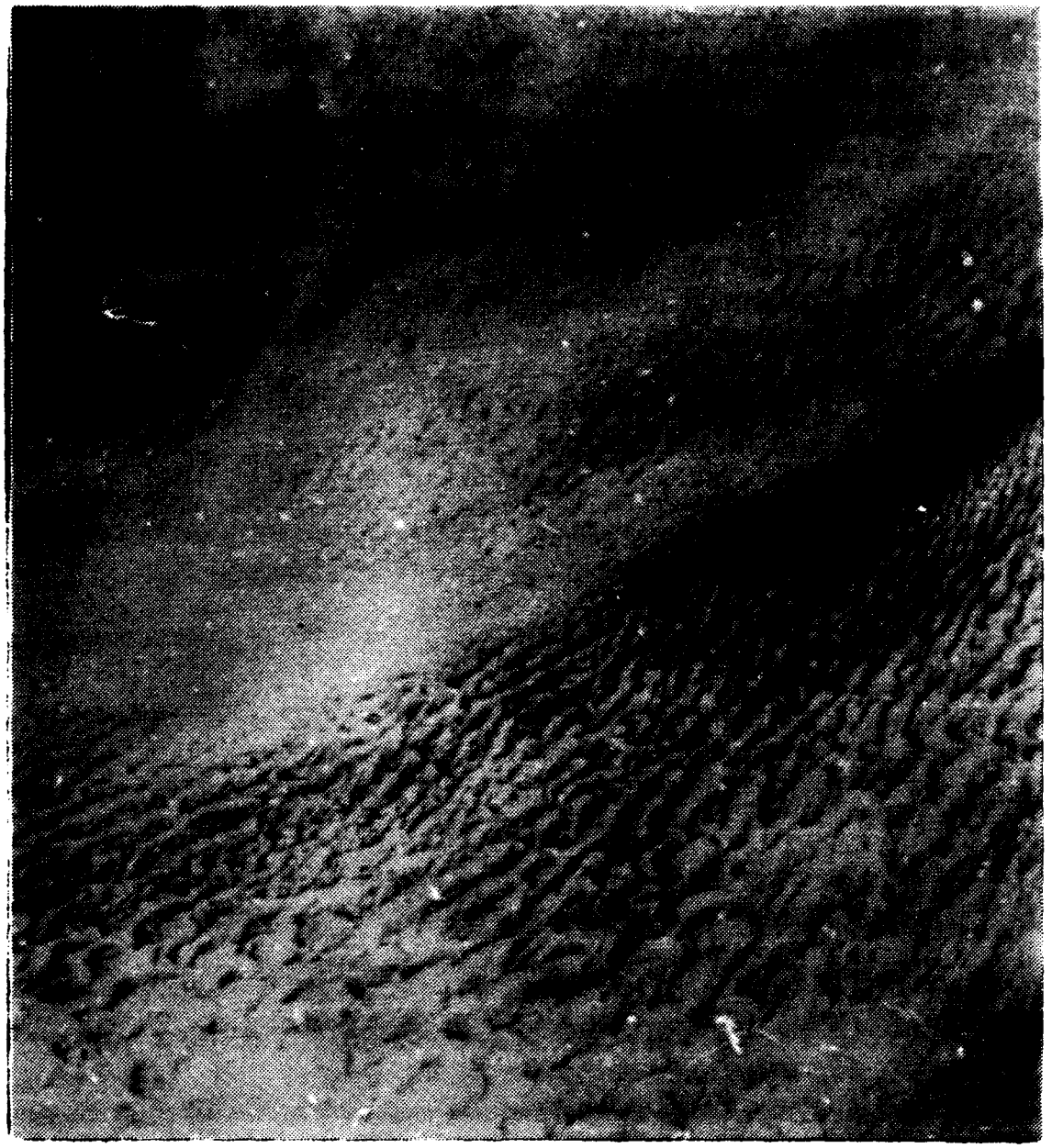

Fig. 15. Case 2 infrared channel 4 satellite imagery: 2314 UTC on 13 July 1987

reflectance modification is used it takes the place of the channel 3 radiance in the detection algorithm. In this case the other tests will still apply with the exception of the channel 3 radiance threshold. No threshold is applied to the channel 3 reflectance. Each of these additional tests will now be discussed in detail.

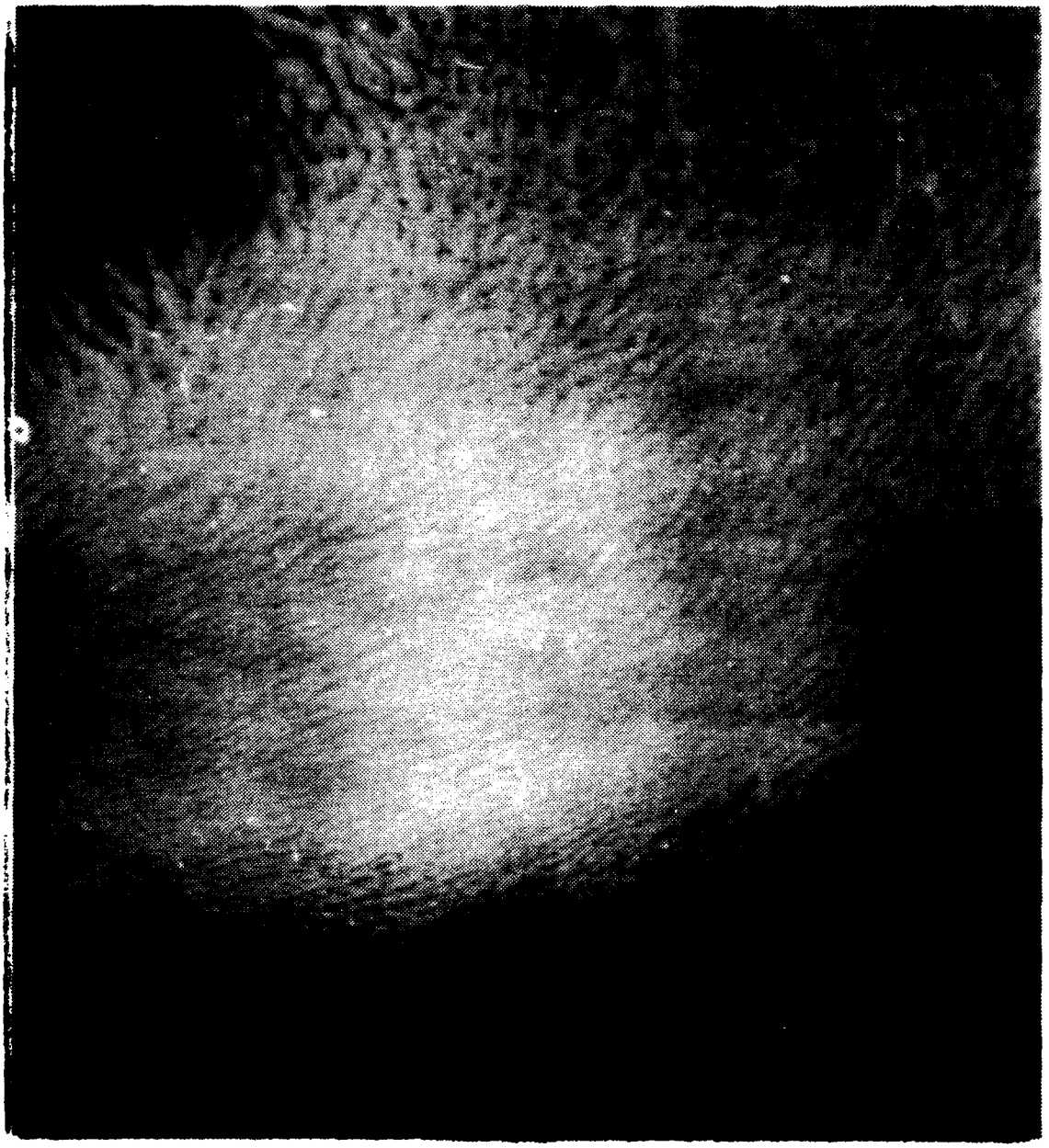

Fig. 16. Case 3 visible channel 1 satellite imagery: 2314 UTC on 13 July 1987

1. Channel 4 Variance Test

This test takes advantage of the fact that the original Coakley algorithm separates each 512 by 512 subscene of data into 64 by 64 subframes. CBD does this to allow the examination of areas small enough to make the assumption that the entire 64 by 64 subframe will have similar cloud properties. This test takes this assumption a step

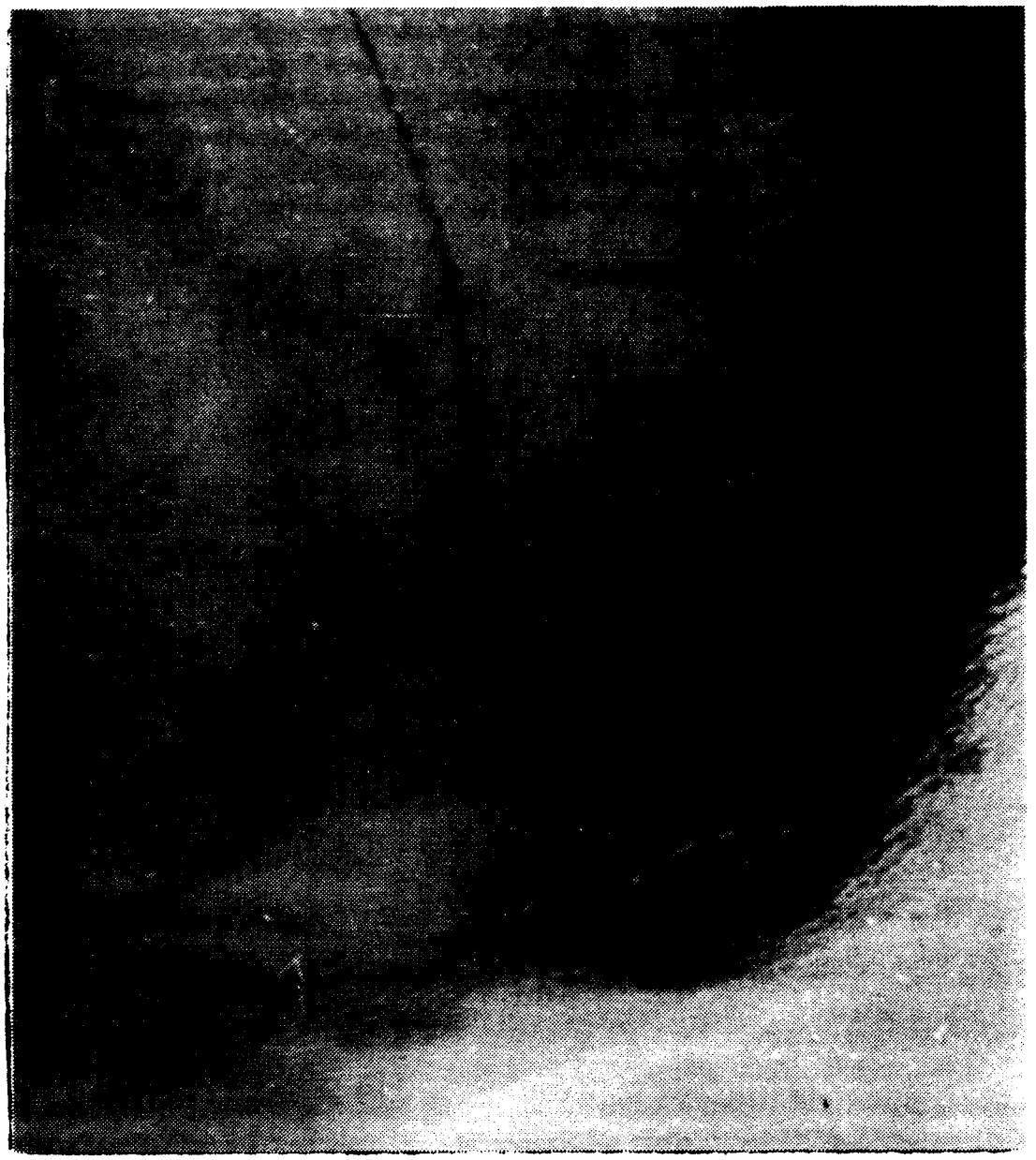

Fig. 17. Case 3 near-infrared channel 3 satellite imagery: 2314 UTC on 13 July 1987

further by allowing the elimination of any subframes which do not exhibit the desired similar cloud properties.

This test examines the channel 4 radiance in each 64 by 64 subframe. A mean radiance value and standard deviation of the channel 4 radiances for each subframe is

Fig. 18. Case 3 infrared channel 4 satellite imagery: 2314 UTC on 13 July 1987

computed. The value of the standard deviation is then compared to an operator supplied cutoff variance. If the computed standard deviation is greater than the cutoff value then the entire subframe is eliminated and assumed to be without ship tracks. This allows areas with dissimilar cloud properties as indicated by thermal infrared properties to be ignored. Examples of regions where the infrared shows a large variability are sharp,

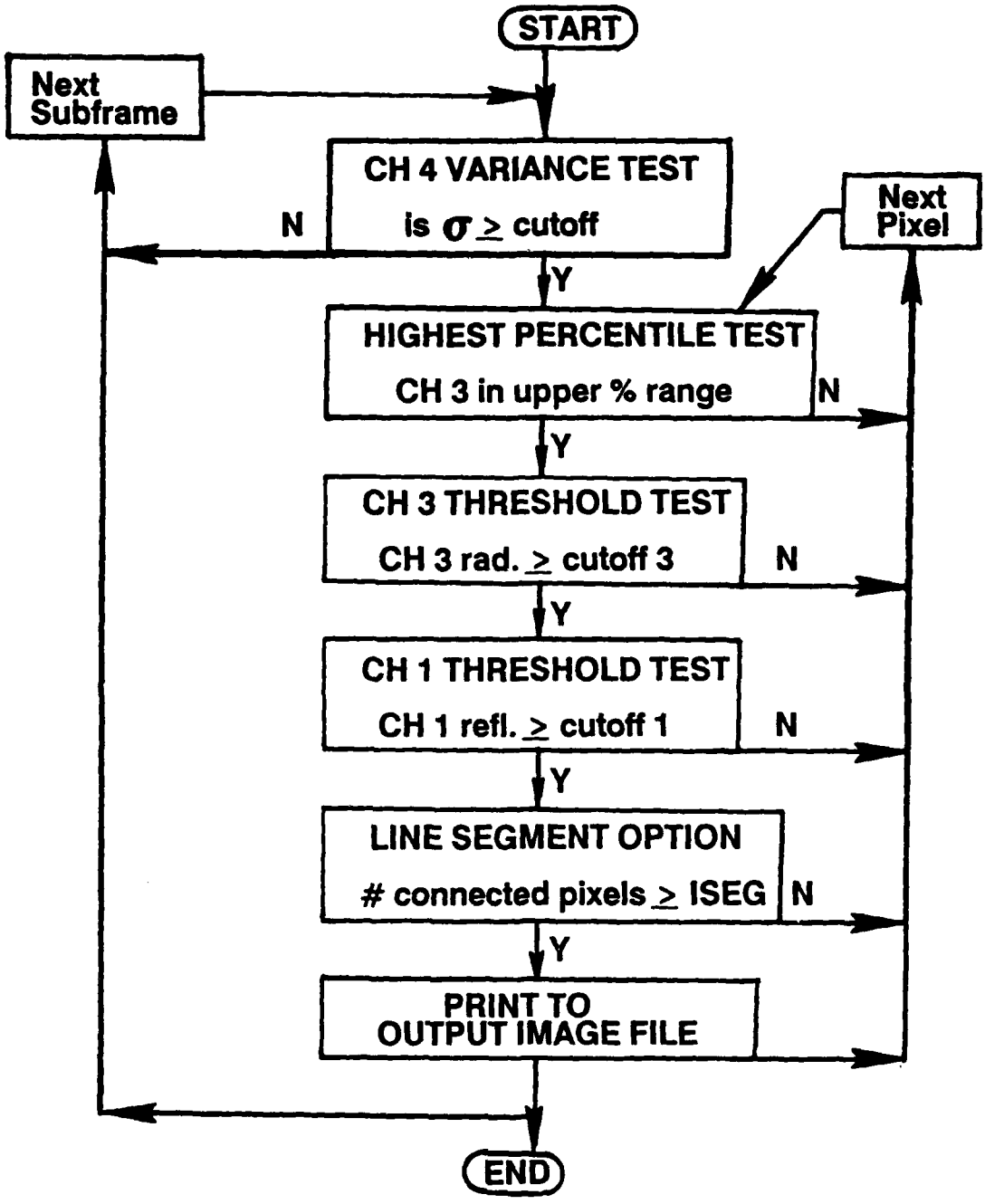

Fig. 19. Ship track detection algorithm testing flowchart.

well defined cloud edges, land areas, and areas representing a transition from one cloud type or regime to another. Since the thermal emission characteristics are not sensitive to the ship tracks (except in cloud free regions) this test is not expected to adversely affect the areas with tracks unless they occur across a sharp cloud boundary.

In this study the value for the standard deviation cutoff is varied from 0.7 to 2.1 in units of radiance in an attempt to determine the best value for eliminating undesired regions without seriously adversely affecting true ship track pixels. Setting the value for the channel 4 variance cutoff to a high value effectively yielded results similar to the original Coakley algorithm and allowed the inclusion of all subframes. When the cutoff was set to 2.1 few, if any, subframes were eliminated. For practical purposes these results were similar to the original algorithm. In the channel 4 imagery (Fig. 15) we can see that the region in the lower portion of the subscene shows considerable variability due to the broken structure of the cloud mass. The channel 3 imagery (Fig. 14) confirms that there are no ship track cloud features in this region. This area represents a transition from the more solid stratiform clouds to the north. The variability in channel 4 can be used to remove some erroneous pixels by using the standard deviation cutoff to 1.1. Fig. 20 shows a case 2 channel 3 satellite image overlayed with ship track pixels generated with the channel 4 variance cutoff set to 1.1 (yellow pixels) and 2.1 (both yellow and red pixels). Fig. 20 shows that many unwanted pixels are generated by the algorithm in the lower portion of the subscene when using the cutoff value of 2.1. By lowering the standard deviation cutoff to 1.1 only the yellow pixels remain. This eliminates the undesirable erroneous pixels shown in red giving a much better representation of the ship track pixels. When this test was applied over a land area, all continental subframes were effectively eliminated.

Decreasing this value further began to eliminate subframes with ship tracks. On the basis of the test cases examined, a standard deviation of approximately 1.1 gave the best results. Many problem areas were eliminated without significant loss of ship tracks.

2. The Channel 1 Threshold Test

This test examines the channel 1 radiance for each pixel which is selected as a potential ship track. The channel 1 reflectance is then compared to a user supplied reflectance threshold. If the reflectance is below the threshold then the pixel is ignored, if it is above the threshold then it is retained as a potential ship track. This test is based on the fact that ship tracks are a cloud feature and therefore will have some minimum

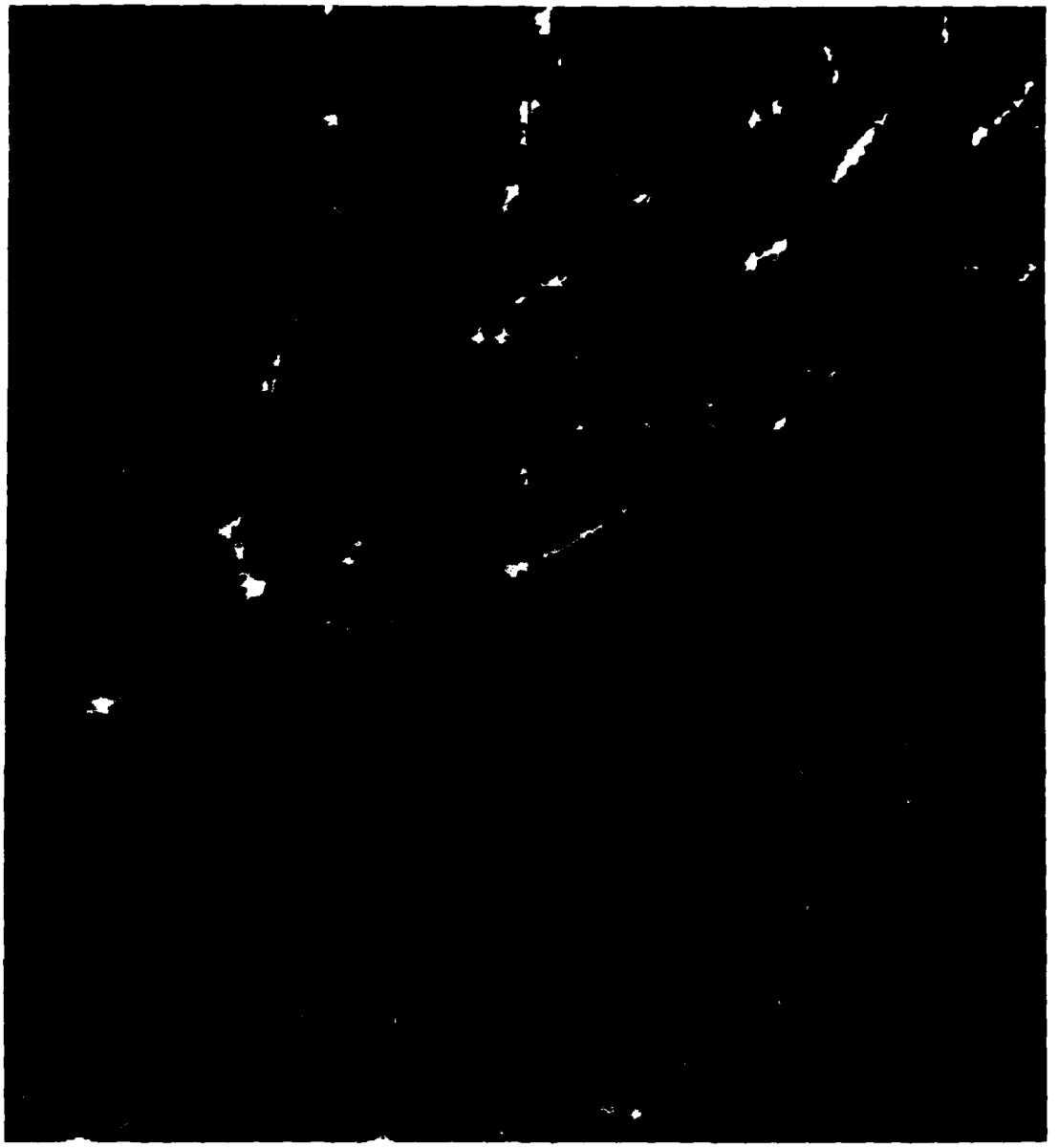

Fig. 20. Channel 4 variance test comparison for case 2: channel 4 variance threshold set to 1.1 (yellow pixels) and 2.1 (yellow and red pixels)

visible reflectance. A low channel 1 value indicates a completely cloud free area and is of no particular interest in this study. Subscenes containing considerable cloud free areas are expected to benefit from this test. The value of the threshold is varied between 12 and 20 percent reflectance to determine the best cutoff for each of the test cases

When placing this threshold between 12 and 15%, most of the prospective ship track pixels pass the test. Only when it is increased to 16-20% does it provide a reasonable measure of improvement. Fig. 21 shows a case 1 channel 3 satellite image overlayed with ship track pixels generated with the channel 1 cutoff set to 12% (red and yellow pixels) and 16% (yellow pixels only). With the threshold at 12% several significant areas of erroneous pixels are generated by the algorithm. Two of these are labeled as A and B in Fig. 21. Raising this threshold to 16% eliminates the red pixels leaving only those in yellow. This completely eliminates the problem pixels labeled A in the figure and produces considerable improvement in the region labeled B. Unfortunately, this increased threshold also shows a slight degradation in the representation of some valid ship tracks.

Cases 1 and 2 have significant areas which are clear as observed in the channel 1 imagery. In these cases this test provides a reasonable degree of improvement. Case 3, which contains a large solid stratus cloud mass, naturally is not improved by this test. This is an expected result since the test is designed to improve cloud free area representation. For case 1 the optimal channel 1 cutoff value was 17% and for cases 2 and 3 a threshold of 20% gave the best results.

3. Channel 3 Threshold Test

This test examines the pixels having channel 3 radiances in the highest percent grouping and then compares them to a user supplied minimum radiance threshold value. If the radiance is below the cutoff value then the pixel is eliminated, if greater than the threshold then the pixel is retained as a potential ship track. The goal of this test is to eliminate the tendency of the program to find ship track pixels in subframes where no ship tracks are present under the assumption that a ship track will have some minimum value of channel 3 radiance. To determine the most feasible value for this threshold, radiances between 0.48 and 0.55 $mW/m^2\text{-}sr\text{-}cm^{-1}$ are tested.

For cases 1 and 3 the channel 3 radiance of the ship track clouds was high enough above the background radiance that this test was not necessary and yielded no positive results. For case 2 its use resulted in only a slight improvement in ship track representation. A high channel 3 cutoff precludes many legitimate ship track pixels whereas lowering the threshold improves the ship track definition but also adds undesired erroneous pixels.

The improvements for case 2 produced by the inclusion of this test were so slight that they could not be effectively shown with a figure, hence none is provided. Again,

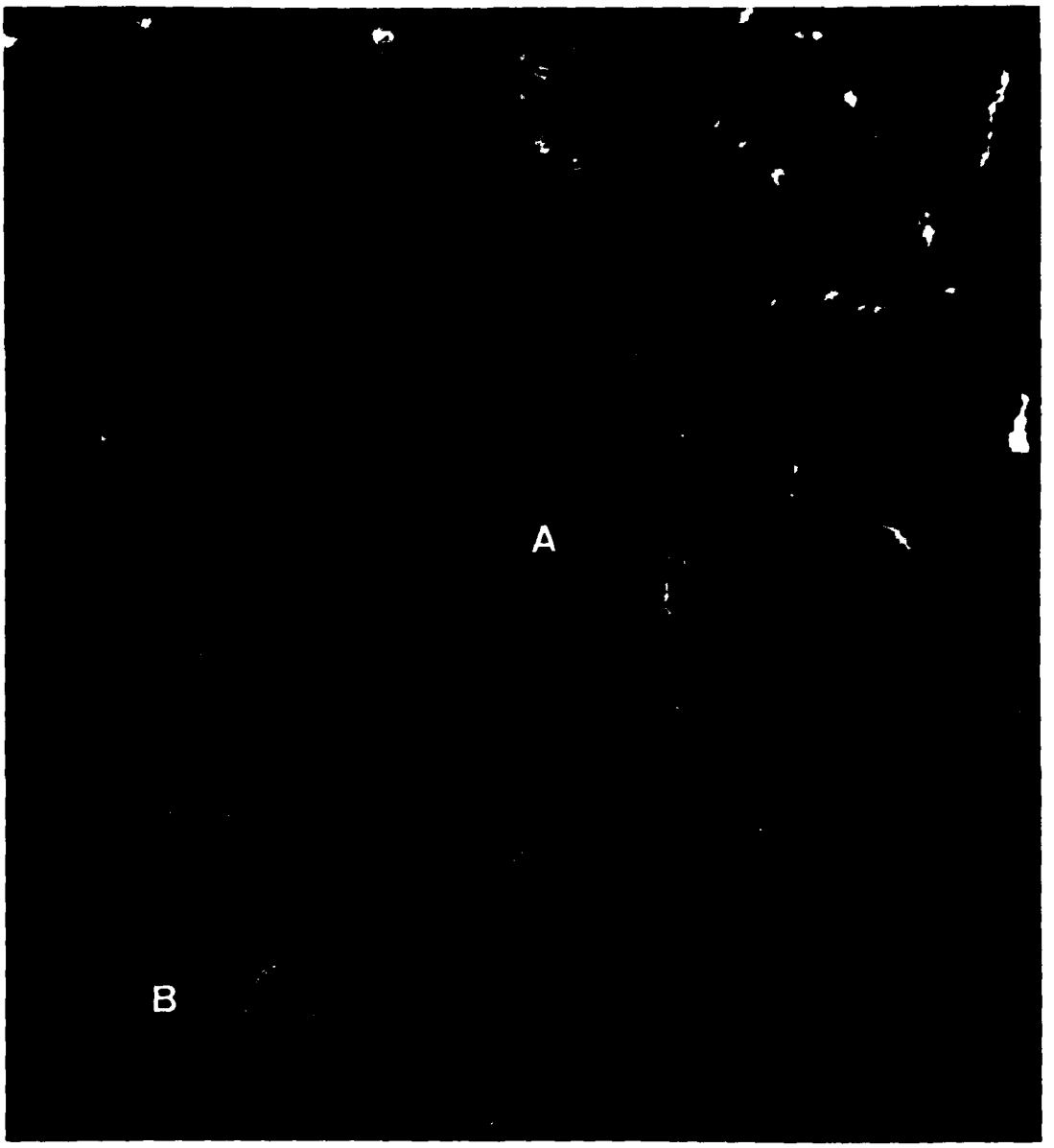

Fig. 21. Channel 1 threshold test comparison for case 1: channel 1 cutoffs of 12% (red and yellow pixels) and 16% (yellow pixels only)

cases 1 and 3 did not respond to this test. The fault with this test appears to lie in the assumption that all ship tracks will have some minimum channel 3 radiance. The radiance of the ship track clouds is highly variable and dependant upon the particular

subframe being examined. This make the selection of a valid threshold value difficult. The best value for this cutoff was 0.5242 mW/m^2-sr-cm^{-1} .

4. Significant Line Segment Option

The significant line segment option allows the number of connected pixels which are considered a ship track cloud to be varied. A large measure of the ability of the algorithm to detect ship tracks while ignoring non-perturbed background clouds rests with this test. The retention of only those pixel groups which demonstrate connectivity is improved by using a high value for this option. This promotes the representation of curvilinear features such as ship tracks. Unfortunately, this makes it very difficult for the algorithm to detect all of a given track. This difficulty is increased as tracks grow older and more diffuse. A low line segment option value allows the broken portions of ship track cloud lines to be represented but also allows the selection of some high radiance pixels which do not exhibit the necessary linear structure of ship tracks. This value is varied between 5 and 13 pixels to determine the value which best represents ship tracks without the inclusion of excessive background pixels.

Fig. 22 shows a case 3 near-infrared image overlayed with ship track pixels produced by setting the line segment option to 5 (yellow and red pixels) and 13 (yellow pixels only). The most striking result drawn from this figure is the relative similarity of the results for widely different line segment options values. When applying the algorithm to case 3, many erroneous pixels are selected for both line segment option values. Setting the value to 13 pixels was expected to eliminate much of this background noise but the results seen in Fig. 22 do not fully support this hypothesis. The number of pixels lost by increasing the segment option to 13, represented by the red pixels in the figure, is roughly equivalent for the ship track and background areas. Hence, while the proper curvilinear structure of the ship tracks is important, it does not appear that the success of the algorithm depends as heavily on this variable as was originally believed. The optimal line segment option value which generally produced the best results in the test cases studied here was 9 pixels.

5. Variation of the Channel 3 Highest Percentile Value

This test allows the number of pixels initially selected as potential ship track pixels to be altered. One of the criteria for selection of the test cases was the availability of ship tracks. As such, each of these cases has a large number of pixels representing tracks. In some areas of these test cases large portions of tracks were not detected by the algorithm. When examining these tracks closely it can be seen that they often cover

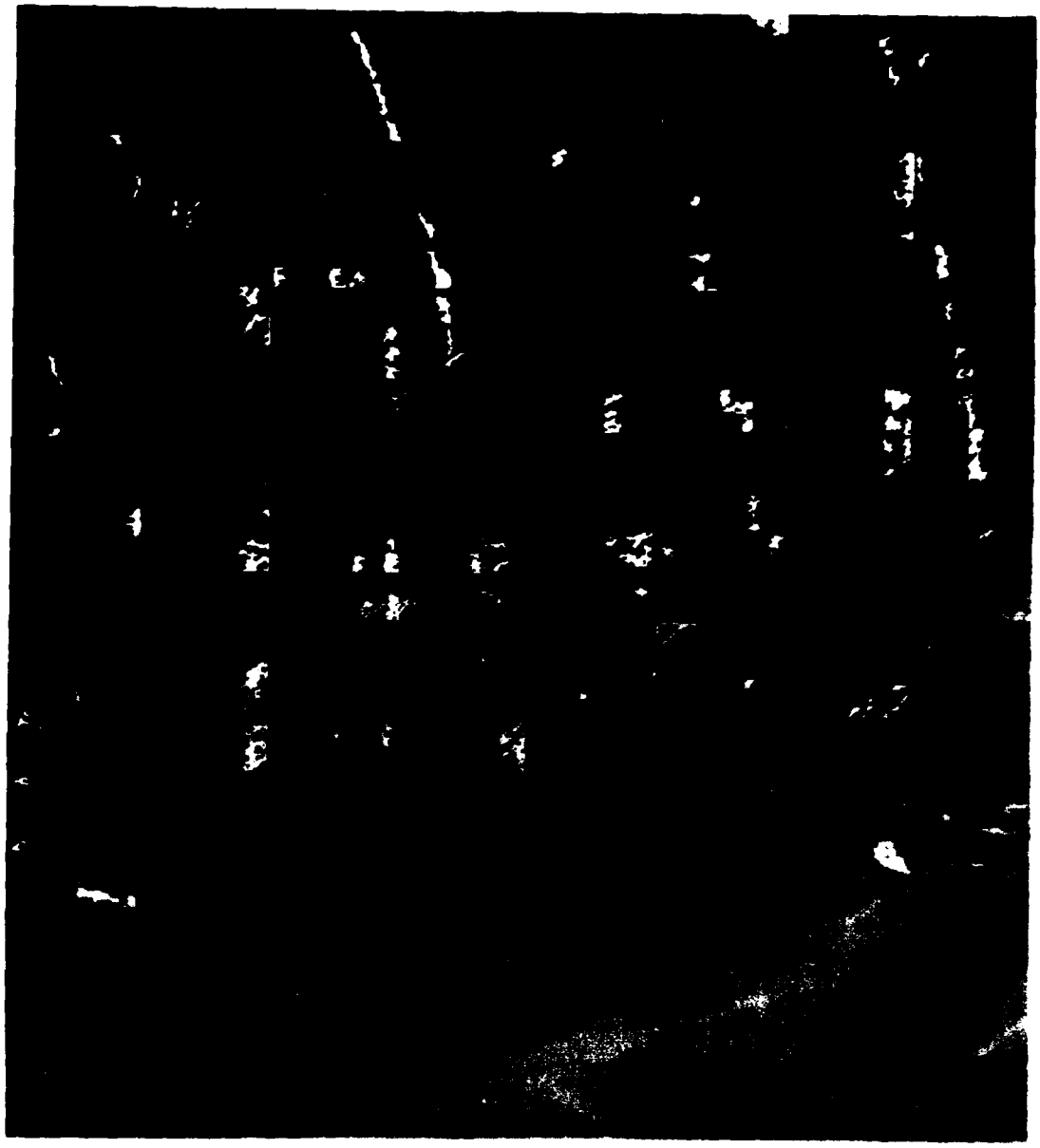

Fig. 22. Significant line segment option comparison test for case 3: line segment values of 5 (yellow and red) and 13 (yellow only) pixels

more that 3.25% of the pixels in the subframe allowed by the Coakley algorithm. This is particularly true in subframes which contain more than one track or an older, more diffuse track. When this occurs it is impossible for the algorithm to fully represent the

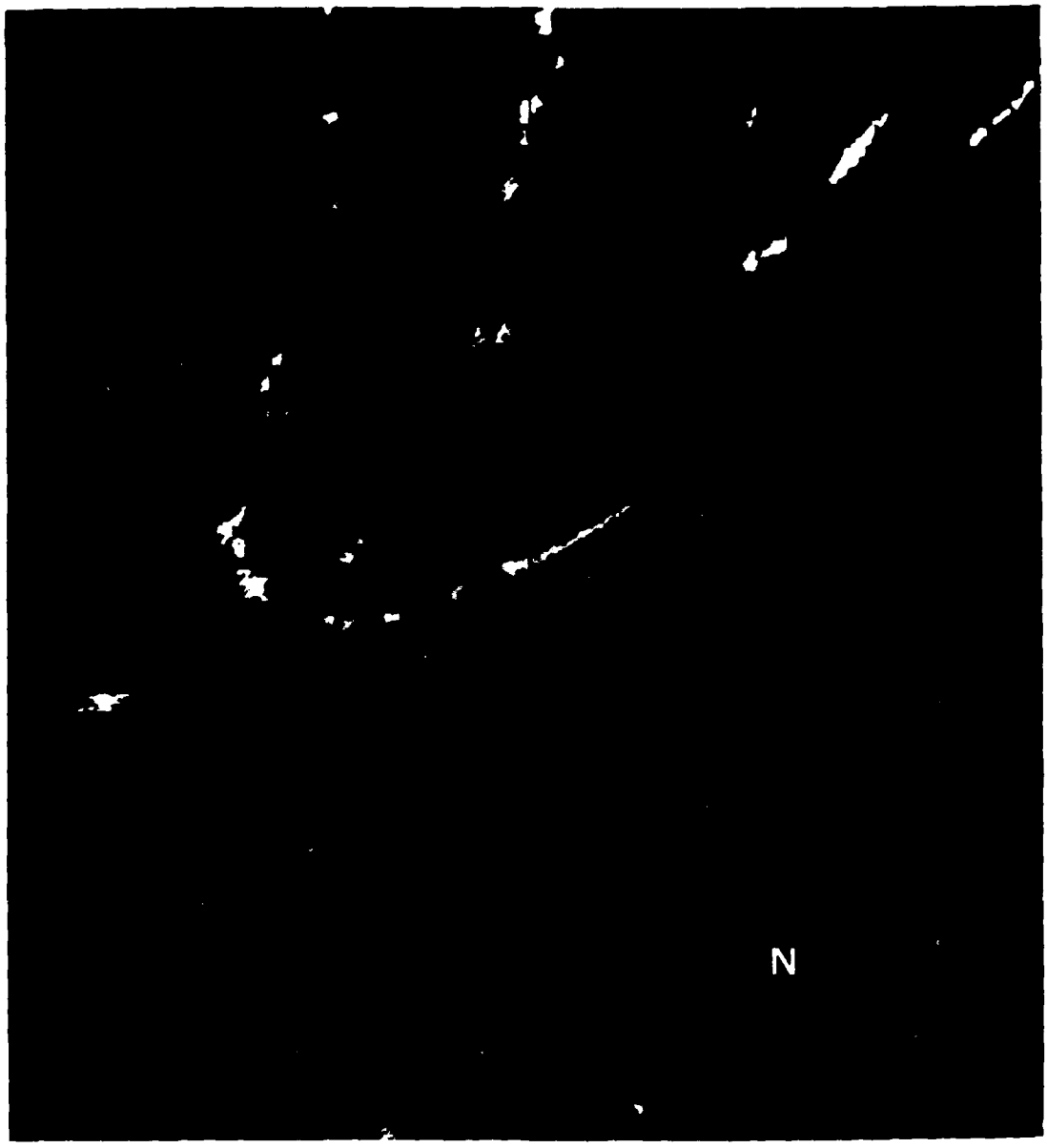

Fig. 23. **Highest percentile value test comparison for case 2:** highest percent values of 3% (yellow pixels) and 10% (yellow and red pixels)

track structure. The accurate representation of these types of regions is only possible if the number of pixels initially examined as potential ship tracks is increased.

In an effort to improve upon this shortcoming in the algorithm, the percentage of pixels considered as potential ship tracks was varied from 3 to 10%. This provided

an easy method of altering the number of potential ship track pixels initially selected. In Fig. 23 the case 2 channel 3 image is shown overlayed with ship track pixels generated for highest percentile values of 3% (yellow pixels) and 10% (yellow and red pixels). Looking at the pixels selected in the 3% case we can see that large portions of all ship tracks are missing. The 10% pixel case (red and yellow pixels) represents more than a threefold increase in pixels selected and results in a much better representation of most of the tracks. Unfortunately there is also an increase in the number of background noise pixels (particularly in the region labeled N on the figure) since some of the pixels not within the highest 3% will fall into the highest 10% grouping. The results for cases 1 and 3 were similar. The value chosen as giving the best results for these test cases was 4%. This is not based so much on a complete representation of the tracks as it is on eliminating unwanted background pixels to the greatest extent possible.

6. Channel 3 Reflectance

The final improvement technique applied to the algorithm is to use a channel 3 reflectance signature rather than the raw channel 3 radiance values used up to this point. As stated in the theory chapter, the near-infrared data contains both reflectance and thermal emittance information. Since the ship exhaust reaches thermal equilibrium relatively quickly, it is likely that the tracks appear as a result of their altering the reflectance portion of channel 3. Channel 3 reflectance is computed pixel by pixel by using the channel 4 radiance values to quantify the temperature effects and subtracting this from the raw channel 3 data. The drawback of this method is that the channel 3 reflectance computation requires a great deal of computer processing time. The results for these tests show that this technique introduces an approximate tenfold increase in the algorithm run time and renders it unusable for a large scale analysis. These results will be presented in the next section.

7. The Best Case Results

The best case results for the first five tests described above are summarized in Table 2.

TABLE 2 Summary of the Best Case Results for each of the Ship Track Algorithm Tests for Test Cases 1, 2 and 3.			
Test Parameter	Case 1 Best Values	Case 2 Best Values	Case 3 Best Values
Channel 4 Variance Test	1.1	1.1	1.1
Channel 1 Threshold Test	17 %	20 %	20 %
Channel 3 Threshold Test	0.5242	0.5242	0.5242
Line Segment Option	9	9	9
Highest Percent Criteria	4 %	4 %	4 %
Units for channel 4 variance test and channel 3 threshold test are $mW/m^2\text{-}sr\text{-}cm^{-1}$			

Each of these values in the table was combined to produce the best case ship track representations shown in Figs. 24, 25 and 26. Each of these figures shows a comparison between the best case results using the channel 3 radiance data (represented by the green and yellow pixels) and those using the channel 3 reflectance (shown by the red and yellow pixels). For all cases it can be seen that using the reflectance information adds to the total number of pixels considered ship tracks. This could be partially due to the loss of the channel 3 threshold test. In case 1 the vertical ship tracks show improvements as some previously blank regions are filled in. Unfortunately there is also an equally significant increase in erroneous ship track pixels randomly distributed about the subscene. Case 2 shows similar results but the enhancement of the ship tracks is proportionally larger than the increase in the erroneous background pixels. For case 3 the reflectance method show almost negligible improvement to the ship tracks while increasing the number of erroneous pixels.

When considering the large increase in computer processing time required to produce the channel 3 reflectance results it is difficult to justify the use of this technique for the slight improvements seen. While this would likely render the algorithm unusable for large scale analysis, the channel 3 reflectance technique still can be utilized to bring improvements in cases where time is not a crucial constraint.

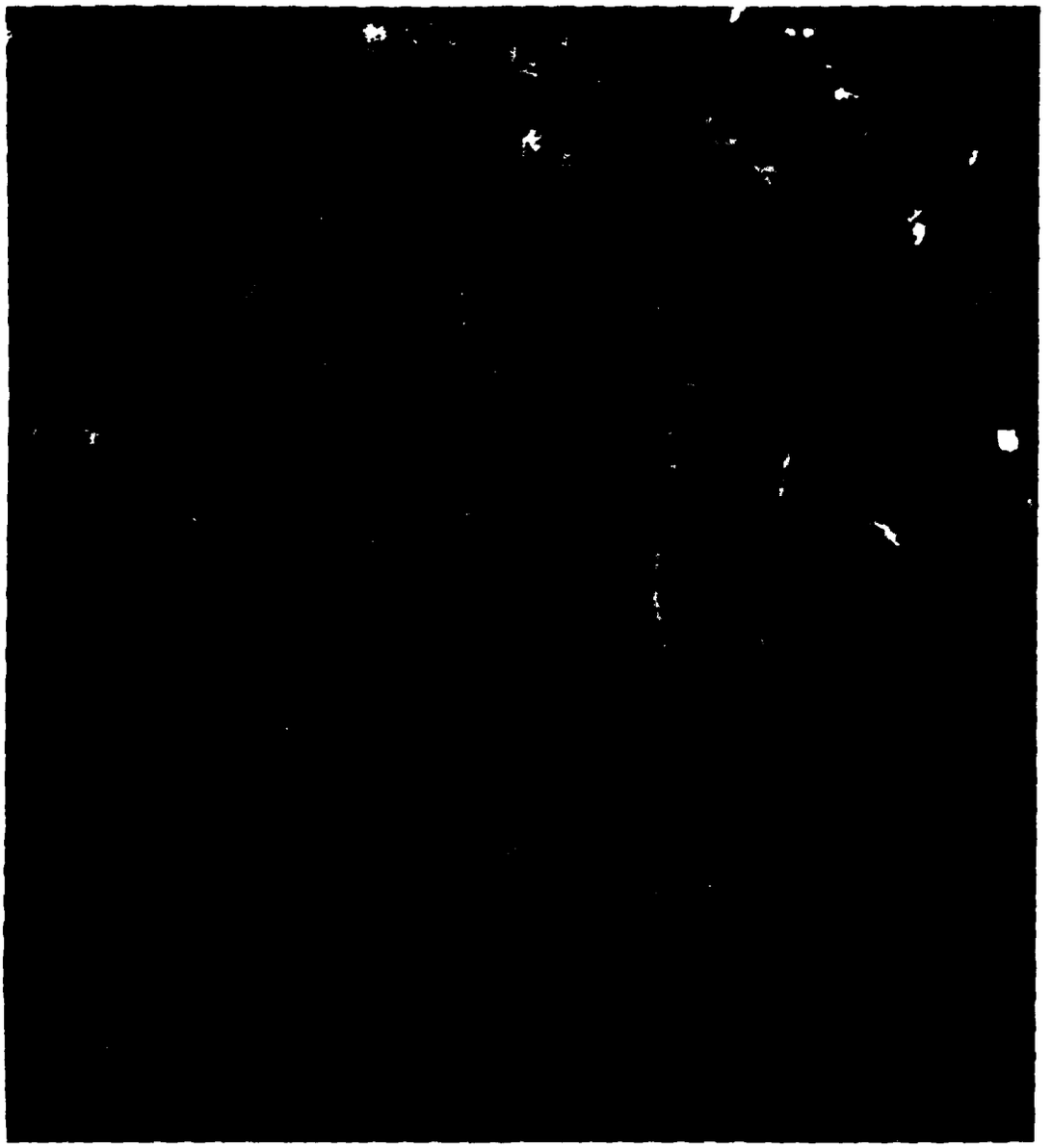

Fig. 24. Comparison of the best ship track images for Case 1: pixels produced using channel 3 radiance are green and yellow, pixels produced from channel 3 reflectance are red and yellow

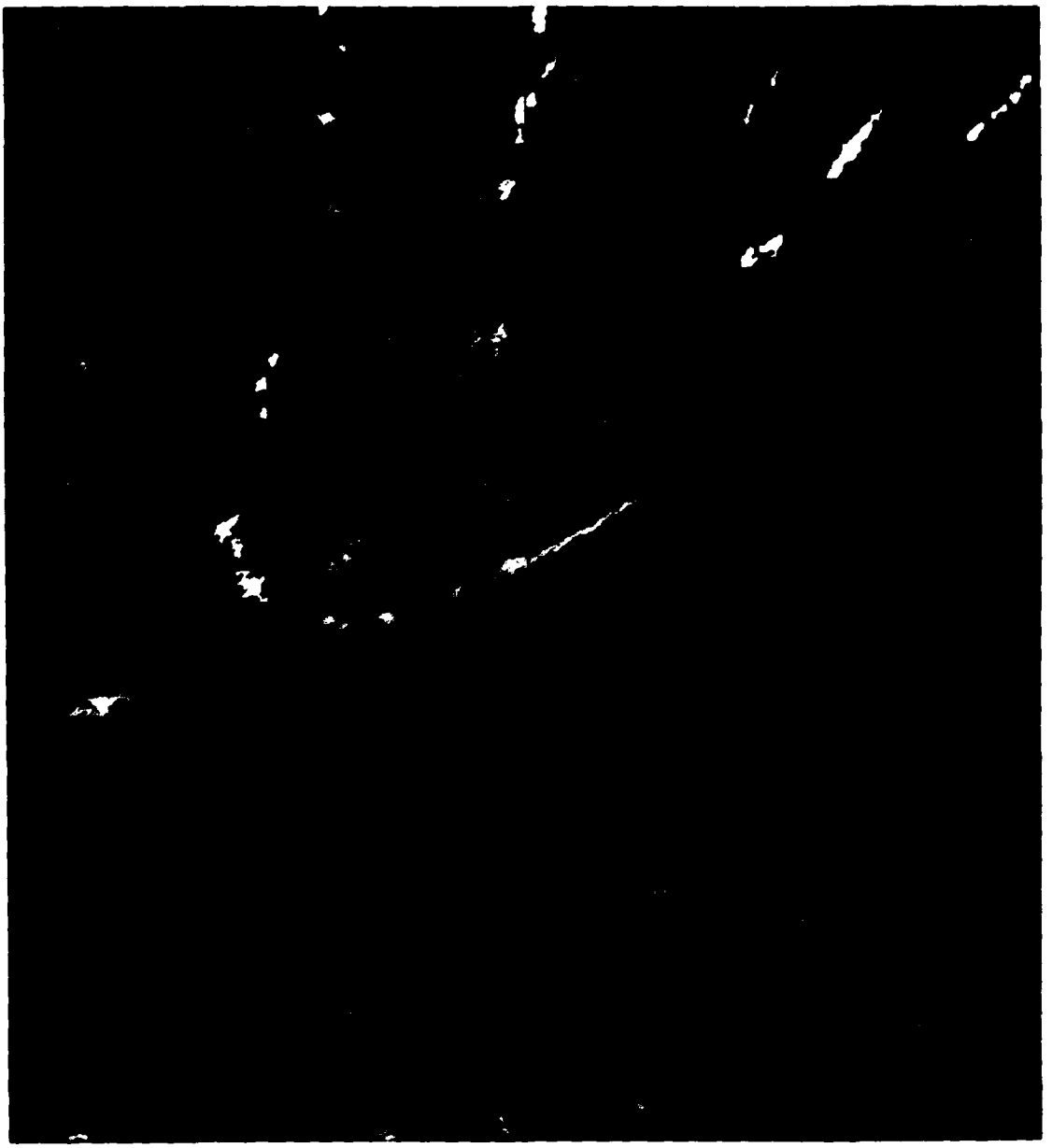

Fig. 25. Comparison of the best ship track images for Case 2: pixels produced using channel 3 radiance are green and yellow, pixels produced from channel 3 reflectance are red and yellow

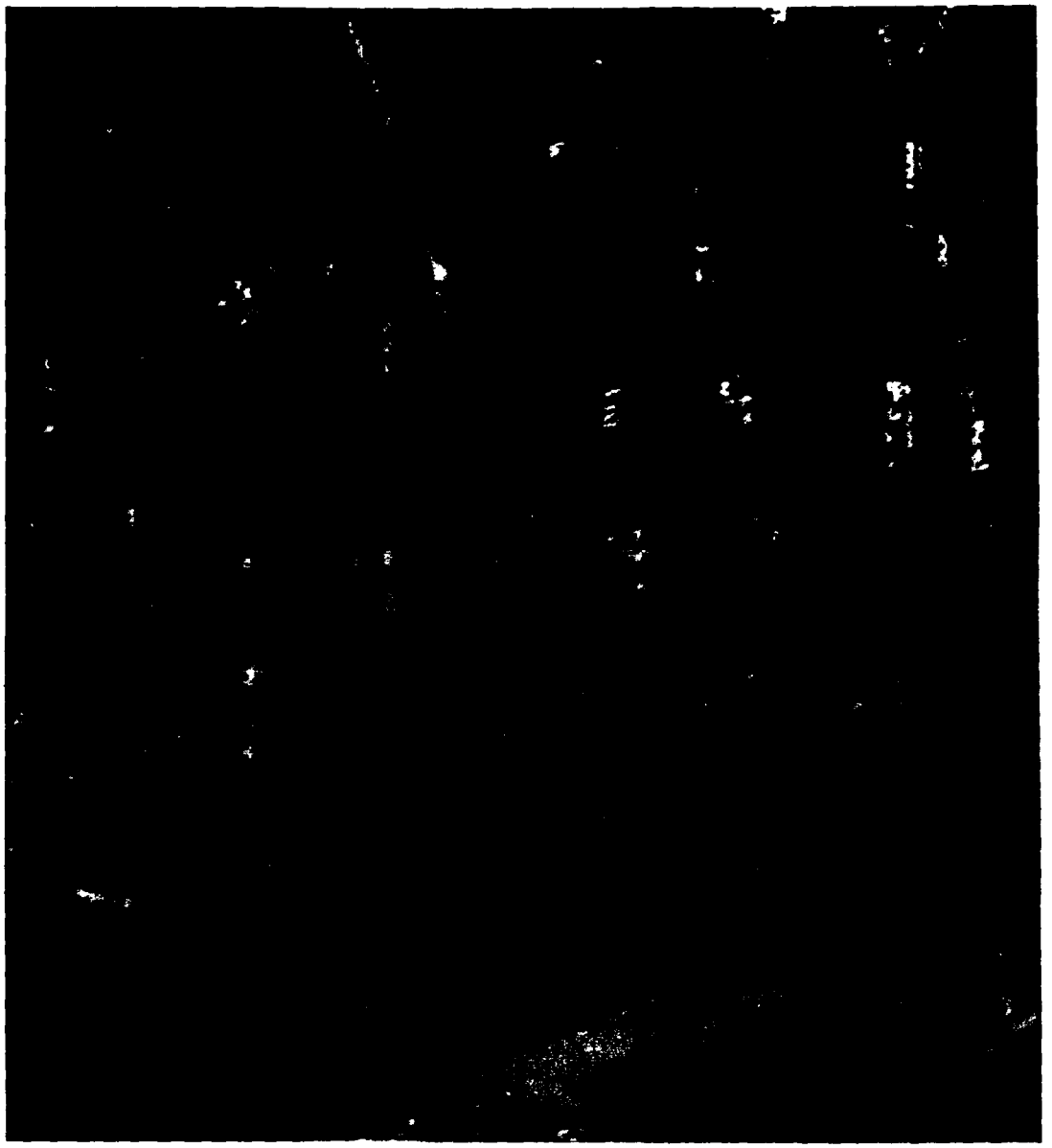

Fig. 26. Comparison of the best ship track images for Case 3: pixels produced using channel 3 radiance are green and yellow, pixels produced using channel 3 reflectance are red and yellow.

TABLE 3 Percent of Pixels Selected by Coakley and Improved Algorithms Which Validate as Ship Tracks			
Case	Total Ship Track Pixels	Valid Ship Track Pixels	% of Pixels That Are Valid Ship Tracks
1 Coakley	6978	1626	23.3
1 Best	1298	768	59.2
2 Coakley	6263	2750	43.9
2 Best	2165	1925	88.9
3 Coakley	6842	1676	24.5
3 Best	3988	1605	40.2

The best case ship track pixel representations of Figs. 24, 25 and 26 are best compared to the results produced by the original Coakley algorithm shown in Figs. 9, 10 and 11 for test cases 1, 2 and 3 respectively. When comparing these figures it is easy to see that while the best case results are not perfect, they do represent a significant improvement over the original detection technique. Table 3 shows the percentage of pixels selected by the Coakley and improved algorithms which validate as ship tracks. In cases 1 and 3 the less than 25% of the ship track pixels selected by the Coakley algorithm were found to be valid ship tracks. The improved algorithm was able to increase this almost 60% for case 1 and to 40% for case 3. For case 1 this represents nearly triple the percentage of valid ship track pixels as the original algorithm. The detection algorithm clearly gave the best results in case 2. In this case, use of the improved algorithm resulted in almost 90% of the pixels selected validating as ship tracks. In each case the percent of valid tracks for the best case is greater than that of the original algorithm.

VI. CONCLUSIONS AND RECOMMENDATIONS

The primary goal of this thesis was to generalize the work of CBD in the development of a ship track detection algorithm. The most important aspects of this effort were to propose and evaluate improvements to the algorithm originally developed in CBD and to expand the technique to analyze large scale areas of data. These objectives are vital to the formation of a globally or regionally applicable ship track detection scheme.

In moving toward these objectives, the results of this thesis are a qualified success. Six potential improvements were applied to the original detection algorithm. With the exception of the channel 3 radiance threshold test, all the new elements in the detection scheme provided some measure of improvement in the results. Fig. 20 through Fig. 23 show the impact of including the following tests to the detection algorithm:

- channel 4 variance test,
- channel 1 threshold test,
- line segment option and
- highest percent category.

The best results for each of these are combined to produce the best case images shown in Figs. 24, 25 and 26. By comparing these figures to the results of the original Coakley algorithm (Figs. 9, 10 and 11) the extent of the improvement to the detection technique can be seen. These improvements are displayed quantitatively in Table 3 which indicates at least a doubling in the ability of the algorithm to select valid ship track pixels. This is particularly significant since the 3 test cases examined were chosen as particularly challenging to the algorithm. Other, less challenging, cases could yield even better results.

While significant improvements in the ability to detect ship tracks have been presented, it is also clear that the results are less than perfect. In none of the cases presented here are all of the valid ship track pixels represented. This is seen in the case 1 results (Fig. 24) which leave many small tracks completely undetected. On the other hand the algorithm still erroneously designates many pixels as ship tracks which clearly do not form anomalous cloud lines. This effect is seen in case 3 which has many pixels of this type (Fig. 26).

The actual detection of ship track cloud features is still best accomplished manually. The ability of the human mind to quickly analyze and evaluate large quantities of data for details such as ship tracks far exceeds the present capability of any automated analysis algorithm. Unfortunately, manual detection of ship tracks introduces the errors associated with subjectivity of the analyzer. As a direct result of this subjectivity, automated and objective techniques like those examined here play an important role in the analysis of ship track data.

The development of a globally usable cloud algorithm is a difficult and complex task. Understanding the role ship track clouds play in the earth's cloud structure is only a small part of this problem. However, it does present a number of issues that must be solved and is worthy of further research. Some of the problems that are within reach of a solution and logically follow from this work are described here.

In keeping with the goal to develop a climatology of ship track occurrence for the North Pacific Ocean using AVHRR data, an attempt was made to apply the ship track detection algorithm to large scale areas. However, the algorithm was not ready for general application to a large area. Part of the reason for this is that the microphysical properties of cloud masses vary considerably over large scale areas. There is still a great deal of work needed in this area before the subject can be considered well understood.

Some specific suggestions for future study are:

1. Perform an in-depth study of the synoptic conditions existing in areas where ship track clouds occur. Determine what conditions are supportive of ship track formation and what elements cause them to be unlikely. This would allow the prediction of areas where ship tracks are likely making their tactical exploitation a better possibility.

2. Attempt to find a ship which is known to have caused the formation of ship tracks and which took meteorological observations during its transit. This will provide an opportunity to examine the in situ conditions and soundings present within ship track clouds.

3. Examine the possible contributions to naval warfare from the development of a useful ship track detection algorithm. This would include the benefits derived from having an accurate means of evaluating the global distribution of cloud cover.

4. Examine the frequency of occurrence for ship track clouds in the region off the North Pacific coast of the United States to determine the most feasible approach to use in developing the ship track climatology.

5. Examine the Atlantic coast of the United States and other ocean regions to determine if the dynamics behind track formation are the same as in the Pacific Ocean.

6. Work to improve the efficiency of the ship track detection program so that it becomes feasible to apply it to the large scale areas required by a climatological study.

Once some of the difficulties with the algorithm are understood and solutions are found, the detection algorithm can be improved. These improvements will allow the use of the technique for forming the climatology needed to more fully understand ship track cloud occurrence. As stated previously this is one small step towards the development of a globally applicable cloud detection and classification algorithm. The development of an acceptable cloud algorithm will be a major milestone in our understanding of the earth's radiation budget.

LIST OF REFERENCES

Allen, R. C., Jr., 1987: Automated satellite cloud analysis: A multispectral approach to the problem of snow/cloud discrimination. M.S. thesis, Naval Postgraduate School, Monterey, CA, May 1987, 66 pp.

Barkstrom, B. R., 1984: The Earth Radiation Budget Experiment (ERBE). *Bull. Amer. Meteor. Soc.*, **65**, 1170-1185.

Coakley, J. A., Jr., R. L. Bernstein and P. A. Durkee, 1987: Effect of ship stack effluents on cloud reflectivity. *Science*, **237**, 953-1084.

Coakley, J. A., Jr., R. D. Cess and F. B. Yurevich, 1983: The effect of tropospheric aerosols on the earth's radiation budget: a parameterization for climate models. *J. Atmos. Sci.*, **40**, 116-138.

Coakley, J. A., Jr., and R. Davies, 1986: The effect of cloud sides on reflected solar radiation as deduced from satellite observations. *J. Atmos. Sci.*, **43**, 1025-1035.

Conover, J. H., 1969: New observations of anomalous cloud lines. *J. Atmos. Sci.*, **24**, 1153-1154.

Durkee, Philip A., 1984: The relationship between marine aerosol particles and satellite-detected radiance. Atmospheric Science Paper No. 380, Department of Atmospheric Sciences, Colorado State University, Fort Collins, CO, 124 pp.

Fett, R. W., P. E. La Violette, M. Nestor, J. W. Nickerson and R. Rabe, (1979): Navy tactical applications guide. volume II, environmental phenomena and effects. Department of the Navy, Washington, D. C., NEPRF Technical Report 77-04, 161 pp.

Henderson-Sellers, A., 1984: Satellite sensing of a cloudy atmosphere: observing the third planet. Taylor and Francis, London, 340 pp.

Hindman, E. E., II, P. V. Hobbs and L. F. Radke, 1977: Cloud condensation nucleus size distributions and their effects on cloud droplet size distributions. *J. Atmos. Sci.*, **34**, 951-956.

Houghton, H. G., 1954: On the annual heat balance of the northern hemisphere. *J. Meteorol.*, **11**, 1-9.

Hunt, G. E., 1972: Radiative properties of terrestrial clouds at visible and infra-red thermal window wavelengths. *Quart. J. R. Met. Soc.*, **99**, 346-369.

Liou, K. N., 1980: An introduction to atmospheric radiation. Academic Press, New York, 392 pp.

Rossow, W. B., F. Mosher, E. Kinsella, A. Arking, M. Desbois, E. Harrison, P. Minnis, E. Ruprecht, G. Seze, C. Simmer, and E. Smith, 1985: ISCCP cloud algorithm intercomparison. *J. Climate Appl. Meteor.*, **24**, 877-903.

Shettle, E. P. and R. W. Fenn, 1979: Models for the aerosols of the lower atmosphere and the effects of humidity variations on their optical properties. AFGL-TR-79-0214 Air Force Geophysics Laboratories, Hanscom AFB, MA.

Schiffer, R. and W. B. Rossow, 1983: The international satellite cloud climatology project (ISCCP): the first project of the world climate research programme. *Bull. Amer. Meteor. Soc.*, **76**, 779-784.

Stern, A. C., H. C. Wohlers, R. W. Boubel, and W. P. Lowry, 1973: Fundamentals of air pollution. Academic Press, New York, 492 pp.

Twomey, S., 1977: The influence of pollution on the shortwave albedo of clouds. *J. Atmos. Sci.*, **34**, 1149-1152.

Twomey, S. and T. Cocks, 1982: Spectral reflectance of clouds in the near-infrared: comparison of measurements and calculations. *J. Meteor. Soc. Japan*, **60**, 583-592.

Twomey, S., H. B. Howell and T. A. Wojciechowski, 1968: Comments on "anomalous cloud lines". *J. Atmos. Sci.*, **25**, 333-334.

Twomey, S., M. Piepgrass and T. L. Wolfe, 1984: An assessment of the impact of pollution on global cloud albedo. *Tellus*, **36B**, 356-366.

Twomey, S. and J. Warner, 1967: Comparison of measurements of cloud droplets and cloud nuclei. *J. Atmos. Sci.*, **24**, 702-703.

Vonder Haar, T. H., and V. E. Suomi, 1971: Measurements of the earth's radiation budget from satellites during a five year period. part I: extended time and space means. *J. Atmos. Sci.*, **28**, 305-314.

INITIAL DISTRIBUTION LIST

		No. Copies
1.	Defense Technical Information Center Cameron Station Alexandria, VA 22304-6145	2
2.	Library, Code 0142 Naval Postgraduate School Monterey, CA 93943-5002	2
3.	Chairman (Code 63Rd) Department of Meteorology Naval Postgraduate School Monterey, CA 93943-5000	1
4.	Chairman (Code 68Co) Department of Oceanography Naval Postgraduate School Monterey, CA 93943-5000	1
5.	Professor Philip A. Durkee (Code 63De) Department of Meteorology Naval Postgraduate School Monterey, CA 93943-5000	2
6.	Professor Carlyle H. Wash (Code 63Wx) Department of Meteorology Naval Postgraduate School Monterey, CA 93943-5000	2
7.	Dr. James A. Coakley, Jr. National Center for Atmospheric Research Boulder, CO 80307	1
8.	Lt. Steven E. Morehead, USN 16231 Nassau Lane Huntington Beach, CA 92649	1
9.	Director Naval Oceanography Division Naval Observatory 34th and Massachusetts Avenue NW Washington, DC 20390	1
10.	Commander Naval Oceanography Command NSTL Station Bay St. Louis, MS 39522	1

11. Commanding Officer — 1
Naval Oceanographic Office
NSTL Station
Bay St. Louis, MS 39522

12. Commanding Officer — 1
Fleet Numerical Oceanography Center
Monterey, CA 93943

13. Commanding Officer — 1
Naval Environmental Prediction Research Facility
Monterey, CA 93943

14. Chairman, Oceanography Department — 1
U. S. Naval Academy
Annapolis, MD 21402

15. Chief of Naval Research — 1
800 North Quincy Street
Arlington, VA 22217

16. Office of Naval Research (Code 420) — 1
Naval Ocean Research and Development Activity
800 North Quincy Street
Arlington, VA 22217